



VICTORIA UNIVERSITY
MELBOURNE AUSTRALIA

Diffusion behavior of humic acid during desalination with air gap and water gap membrane distillation

This is the Accepted version of the following publication

Amaya-Vías, D, López-Ramírez, JA, Gray, Stephen, Zhang, Jianhua and Duke, Mikel (2019) Diffusion behavior of humic acid during desalination with air gap and water gap membrane distillation. *Water Research*, 158. pp. 182-192. ISSN 0043-1354

The publisher's official version can be found at
<https://www.sciencedirect.com/science/article/pii/S0043135419302787>
Note that access to this version may require subscription.

Downloaded from VU Research Repository <https://vuir.vu.edu.au/38403/>

1 Diffusion behavior of humic acid during desalination with air gap and
2 water gap membrane distillation

3 David Amaya-Vías¹, Juan A. López-Ramírez¹, Stephen Gray², Jianhua Zhang², Mikel Duke^{2*}

4 ¹Departamento de Tecnologías del Medio Ambiente, Faculty of Marine and Environmental
5 Sciences. Instituto Universitario de Investigación Marina (INMAR). Campus de Excelencia
6 Internacional del Mar (CEIMAR). University of Cadiz, Puerto Real, 11510 Cádiz. Spain

7 ²Institute for Sustainable Industries and Liveable Cities, Victoria University, Melbourne, PO
8 Box 14428, Victoria 8001, Australia

9 Corresponding author: Mikel Duke

10 E-mail: mikel.duke@vu.edu.au

11

12 **Abstract**

13 Desalination and water reuse are important means to resolve local water scarcity and security
14 issues worldwide where membrane distillation (MD) may be part of a solution. Natural organic
15 matter and in particular, humic acids (HA), are widely present in water supplies to be treated but
16 exhibit little understood behavior to diffuse through MD membranes into permeate. In this
17 work, air gap (AGMD) and water gap (WGMD) were utilized to study HA behavior in MD
18 using seawater and synthetic water over a range of typical MD temperatures, flow rates and
19 membrane types. HA diffusion was first shown with seawater feed then on synthetic solutions at
20 all process conditions. While electrical conductivity rejection was always above than 99%, HA
21 rejection showed values of 33% and 90% for AGMD and 68% and 93% for WGMD with
22 seawater and synthetic water, respectively. Analytical techniques were used to perform a
23 preliminary organic matter characterization in permeate, obtaining clear differences between the
24 feed and permeate HA property. Compared to hydrophobic membranes, uniquely oleophobic
25 membranes inhibit HA diffusion suggesting hydrophobic surface diffusion of HA through the
26 membrane. HA flux as well as potential undesirable effects of the organic matter in permeate
27 should be considered for MD applications.

28 **Keywords:** humic acid, air gap membrane distillation, water gap membrane distillation, organic
29 matter, diffusion, seawater.

30 **1. Introduction**

31 Water shortages and the loss in water quality are one of the main common global problems
32 humanity faces (Anand et al., 2018; Voulvoulis, 2018). In addition, many anthropogenic
33 compounds that cannot be treated with conventional wastewater treatments can be found in
34 natural waters, posing a significant risk to the environment and to human health (Biel-Maeso et
35 al., 2018; Han et al., 2017; Herce-Sesa et al., 2018; Wagner et al., 2016).

36 Of particular interest in water quality are natural organic matter (NOM) compounds which is
37 present in natural water systems. NOM compounds are derived from the degradation of plants,
38 animals, and microorganisms by chemical, biological and photochemical reactions. Among the
39 compounds making up NOM, humic substances (HS) are important since they are the major
40 carbon pool in the biosphere. Of the NOM presents in natural waters, up to 50% consist of HS
41 and they are the main organic compounds in seawater (Lipczynska-Kochany, 2018; Naidu et al.,
42 2015; Rodríguez et al., 2014).

43 HS are complex and heterogeneous mixtures of a wide range of molecular weight species. The
44 two main categories of HS are fulvic acids (FA) and humic acids (HA), and can be
45 distinguished in function of their solubility at pH 1 where the latter often form colloids because
46 of their large size (Rodríguez et al., 2014; Wagner et al., 2016). Although HS do not cause any
47 known adverse effects for human health, they are undesirable substances in water treatment and
48 they can play a fundamental role as indicators of water quality. HS contributes to odor, color,
49 taste and acidity problems in water supplies. Furthermore, HS, and especially HA, lead to a
50 greater spending on disinfection when chlorination is used as they are precursors of toxic
51 disinfection byproducts (DBPs) such as trihalomethanes (THMs) and haloacetic acids (HAAs)
52 (Liu et al., 2008; Roccaro et al., 2009). Finally, HS have been identified as one of the major
53 compounds responsible for fouling in membrane processes as well as the complexes formation

54 with a multitude of metal ions and organic pollutants promoting the formation of biofilm in
55 water pipes (Bond et al., 2012; Chowdhury et al., 2016; Jermann et al., 2007; Liu et al., 2008;
56 Roccaro et al., 2009). Therefore, HA and its behavior through a new proposed water treatment
57 technology is important to be investigated.

58 Water desalination and reuse technologies have great potential to address the problems
59 associated with water shortages and water quality by use of non-conventional water sources.
60 These desalination technologies are mainly based on membrane and/or thermal processes, or a
61 combination of both in a process train while reuse technologies are mainly based on membrane
62 processes. Some of these technologies are reverse osmosis (RO), electrodialysis, nanofiltration
63 (NF), multiple-effect distillation (MED) and multi-stage flash distillation (MSF). An alternative
64 process combining membranes with thermal desalination is membrane distillation (MD)
65 (Criscuoli and Carnevale, 2015; Ghaffour et al., 2013; Kim and Hong, 2018; Prisciandaro et al.,
66 2016; Ziolkowska and Reyes, 2016). MD is a thermally driven separation using a membrane as
67 a barrier for saline liquid water, while being permeable to fresh water vapor. In this way, the
68 vapor pressure between both sides of this membrane, being microporous and hydrophobic in
69 order to fulfill the liquid barrier and vapor permeable requirement, is the driving force in this
70 separation process.

71 The advantages of MD proposed include the use of small and compact equipment and very low
72 working pressures which could lead to lower material costs and greater process safety compared
73 to other conventional technologies (Alkhudhiri et al., 2012a; Essalhi and Khayet, 2015; Khalifa,
74 2015). Additionally, MD can use low-grade and waste heat as well as alternative energy
75 sources, increasing energy efficiency. In terms of membrane performance, the fouling of the
76 membranes can be lower than in other membrane processes while a very high water quality is
77 produced because of the 100% theoretical rejection of non-volatile components (Alkhudhiri and
78 Hilal, 2017; Guillen-Burrieza et al., 2014). Among MD configurations, commonly investigated
79 modes include direct contact MD (DCMD), air gap MD (AGMD) and water gap MD (WGMD).
80 In DCMD, feed and cooling water are in contact with the membrane surfaces. In this way, the

81 transmembrane flow (membrane flux) is high but there are also high heat losses by conduction.
82 As a result of this setup, obtaining an isolated distillate is not possible, since it is mixed with the
83 cooling water. This is avoided with the AGMD setup as the distillate can be obtained separately
84 from the cooling water, however the drawback is membrane flux is lower than in DCMD.
85 Another configuration, WGMD, emerged as an improvement over these limitations of DCMD
86 and AGMD. In WGMD, the gap is filled with distilled water. This configuration offers an
87 improvement in the permeate flow in comparison with AGMD and it allows a separate distillate
88 to be obtained, unlike DCMD (Francis et al., 2013; González et al., 2017).

89 These MD advantages make it a promising alternative to conventional desalination and water
90 reuse technologies for many environmental and industrial applications (Amaya-Vías et al.,
91 2018; Cui et al., 2018; Silva et al., 2018). Nevertheless, MD is not fully commercialized and
92 implemented by industry (Khayet, 2011; Qtaishat et al., 2009), since many aspects have still not
93 been studied in detail; for example, the effect of organic matter (OM) and HA in the MD
94 process. Many authors have focused their studies on the MD fouling and the HA influence in
95 the rejection of different substances. However, the permeation of HA through the membrane
96 into the permeate has so far only been observed as a side result in these DCMD fouling studies
97 (Han et al., 2017; Khayet et al., 2004; Meng et al., 2014; Naidu et al., 2015, 2014; Wijekoon et
98 al., 2014).

99 In view of their importance and consequences of HA presence in treated water supplies, the
100 reason for the diffusion of this non-volatile molecule of large size into the treated MD permeate
101 is clearly of interest to scientists and engineers. This work is therefore dedicated to explore the
102 behavior of HA through the membrane in AGMD and WGMD configurations with the view to
103 understand its diffusion mechanisms. Studies have been carried out in order to analyze the pure
104 permeate and evaluate the behavior of the HA for different membranes, operating temperatures
105 and flow rates. Different conditions have been studied with synthetic water as well as real
106 seawater from a local seawater source.

107 **2. Materials and methods**

108 *2.1. Reagents and membranes*

109 Synthetic water composition used in this study was set at 1 g L⁻¹ sodium chloride (NaCl)
110 EMSURE® (Merck, Germany), 8 mM (~0.88 g L⁻¹) calcium chloride ≥96% anhydrous (CaCl₂,
111 Sigma-Aldrich), 100 mg L⁻¹ humic acid sodium salt (H16752 Sigma-Aldrich) and deionized
112 water, in order to simulate surface water with a typical OM model, according to Han et al (Han
113 et al., 2017). In addition, real seawater was obtained from Port Phillip (Melbourne, Australia) to
114 study NOM behavior in MD.

115 A hydrophobic, microporous membrane from Ningbo Changqi Porous Membrane Technology
116 Co, Ltd. (Ningbo, China) was used in the MD tests. The membrane consisted of a thin
117 polytetrafluoroethylene (PTFE) active layer (40 μm) on top of a polypropylene (PP) support
118 layer, with a nominal pore size and total thickness of 0.5 μm and 106 μm, respectively.
119 Although this PTFE membrane was used as a reference throughout the study, another three
120 membranes were used in order to study the HA behavior with different materials and membrane
121 characteristics.

122 In this way, a hydrophobic polyethylene (PE) membrane and omniphobic PE membrane without
123 support layer from Aquastill were used, featuring both a nominal pore size of 0.2 μm and
124 thickness of 63 μm and 67 μm, respectively. In addition, a hydrophilic polyurethane (PU)
125 coated hydrophobic PTFE membrane from Australian Textile Mills (ATM) was used. PU layer
126 has a pore size less than 2 nm and the PTFE layer, 0.35 μm with a total membrane thickness of
127 164 μm. Some additional membrane characteristics used in this study are reported elsewhere
128 (Mostafa et al., 2017; Qin et al., 2018; Villalobos García et al., 2018).

129 *2.2. Experimental MD setup*

130 MD testing was conducted in a laboratory system in AGMD and WGMD modes using a similar
131 setup reported elsewhere (Amaya-Vías et al., 2018; Francis et al., 2013; Khalifa, 2015). Briefly,
132 MD system consisted of a co-current flat sheet acrylic membrane module with an effective
133 membrane area of 0.018 m², a feed tank, a cooling tank and two peristaltic pumps (Masterflex®

134 L/S 77800-62, Cole-Parmer). One spacer (thickness = 0.8 mm, porosity = 0.87) was placed on
135 feed side to enhance the turbulence of the feed stream. In addition, for both MD configurations a
136 3 mm gap made with a perforated plate was used to support the membrane and prevent the
137 membrane from possible deformation or damage (Alkhudhiri et al., 2012b; Attia et al., 2017b,
138 2017a; Duong et al., 2016; Khalifa, 2015; Khalifa and Alawad, 2018; Pal and Manna, 2010; Xu
139 et al., 2016). Both tanks were covered to minimize losses by evaporation and a mass balance
140 was calculated for all experiments. A heater (Thermo Scientific Neslab RTE7) and a chiller
141 (PolyScience®) maintained the temperatures configured in the feed and cooling tanks,
142 respectively. The permeate was collected in a measuring cylinder and the permeate flow was
143 measured by the volumetric method, as described by Dow et al. (Dow et al., 2016). A simplified
144 schematic flowsheet is shown in Fig.1.

145 Electrical conductivity (EC) and pH of the water samples were determined using a portable
146 multi meter (Hach HQ40D, Loveland, CO, USA).

147 Several parameters were calculated based on experimental measurements. The first is the
148 permeate flow rate ($L h^{-1}$) used to determine total flux, J ($L h^{-1} m^{-2}$) by Eq. (1):

$$J = \frac{V_{perm}}{A \cdot \Delta t} \quad (1)$$

149 Where V_{perm} is the permeate volume produced in the time interval (L), A is the membrane area
150 (m^2) and Δt is the time interval (h).

151 HA flux, J_{HA} ($mg_{HA} h^{-1} m^{-2}$), with respect to total flux in both MD configurations was also
152 calculated as in Eq. (2), where $[HA]$ is the HA concentration ($mg_{HA} L^{-1}$) in permeate collected
153 over time interval Δt , using the TOC calibration equation to specify the $[HA]$. Limits of
154 detection (LOD) were calculated as $3\sigma_b/m$ where σ_b is the standard deviation of ten blank
155 samples and m the slope of the calibration curve. Additionally, limit of quantification (LOQ)
156 was calculated as $10\sigma_b/m$ (Miller et al., 2002).

157

$$J \tag{2}$$

158 Finally, rejection factor (RF) for a variable was calculated by Eq. (3):

159

$$\text{—————} \tag{3}$$

160 Where C_{feed} and C_{perm} are values in the feed and permeate, respectively. This equation was used
161 to calculate the EC rejection factor (RF_{EC}) and Non Purgeable Organic Carbon (NPOC)
162 rejection factor (RF_{NPOC}) using experimentally obtained EC and NPOC values respectively.

163 For the experimental design, real seawater was tested with the purpose of checking the presence
164 of NOM in MD permeate. It was decided to use seawater for two main reasons. Firstly, seawater
165 desalination is one of the main applications in which MD can be potentially used. Secondly,
166 taking into account that HS are the main component of the NOM in seawater (Naidu et al.,
167 2015; Rodríguez et al., 2014), HA flux can be evaluated easily, assuming that all NOM in
168 seawater samples was HA. Therefore, HA flux is estimated by the TOC-HA calibration curves
169 used for synthetic water. Then to ensure tests with a consistent feed, the seawater was replaced
170 with a synthetic saline water in order to study the influence of the both sides (feed and cooling)
171 temperatures, operation flow rates and the different membranes described previously. The initial
172 feed volume was 2.5 L and the operation time for each test was 4 h being sufficient time to
173 show steady state performance. Permeate samples were taken every hour, while feed side was
174 monitored taking a sample at the start and at the end of the test. New membranes were used for
175 each operating condition.

176 Firstly, AGMD and WGMD tests were performed at different temperatures, flow rates and cross
177 flow velocity (CFV) using four different MD membranes as indicated in Table 1.

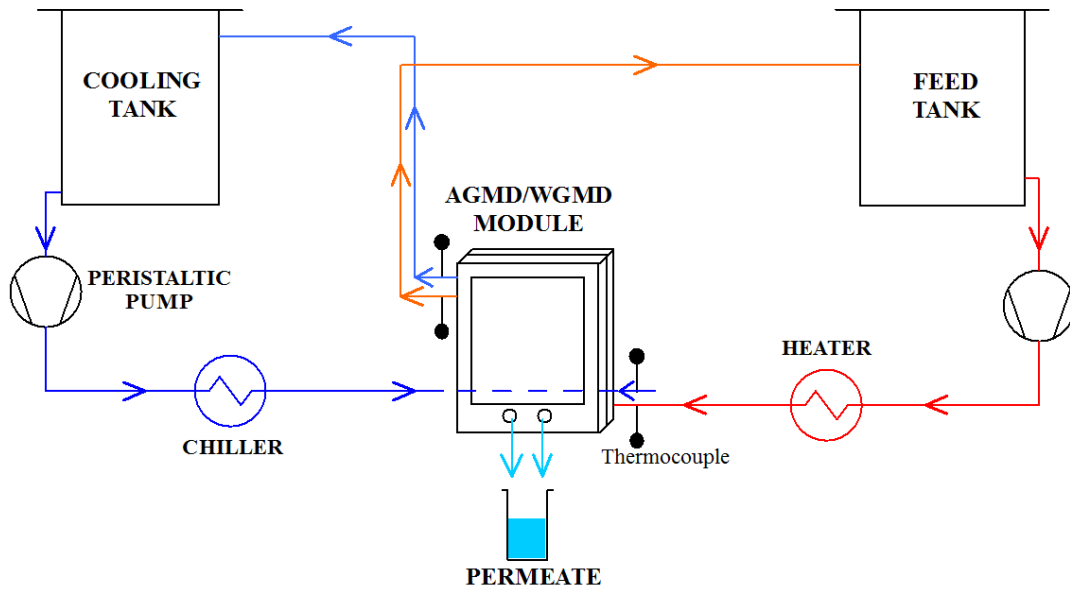
178 **Table 1.** Operating conditions (temperatures, flow rates, CFV and MD membranes) studied in
 179 AGMD and WGMD tests.

Temperature tests at 90 L h⁻¹ (0.034 m s⁻¹) cross flow using PTFE membrane				
Feed temperature (°C) / Cooling temperature (°C)				
50 / 18	60 / 18	70 / 18	70 / 35	
Flow rate tests at 70°C (feed) and 18°C (permeate) using PTFE membrane				
Flow rate (L h ⁻¹) / CFV (m s ⁻¹)				
60 / 0.023	75 / 0.029	90 / 0.034	105 / 0.04	120 / 0.046
Membrane tests at 70°C (feed), 18°C (permeate) and 90 L h⁻¹ (0.034 m s⁻¹) cross flow				
PTFE	PTFE-PU	PE-hydrophobic	PE-omniphobic	

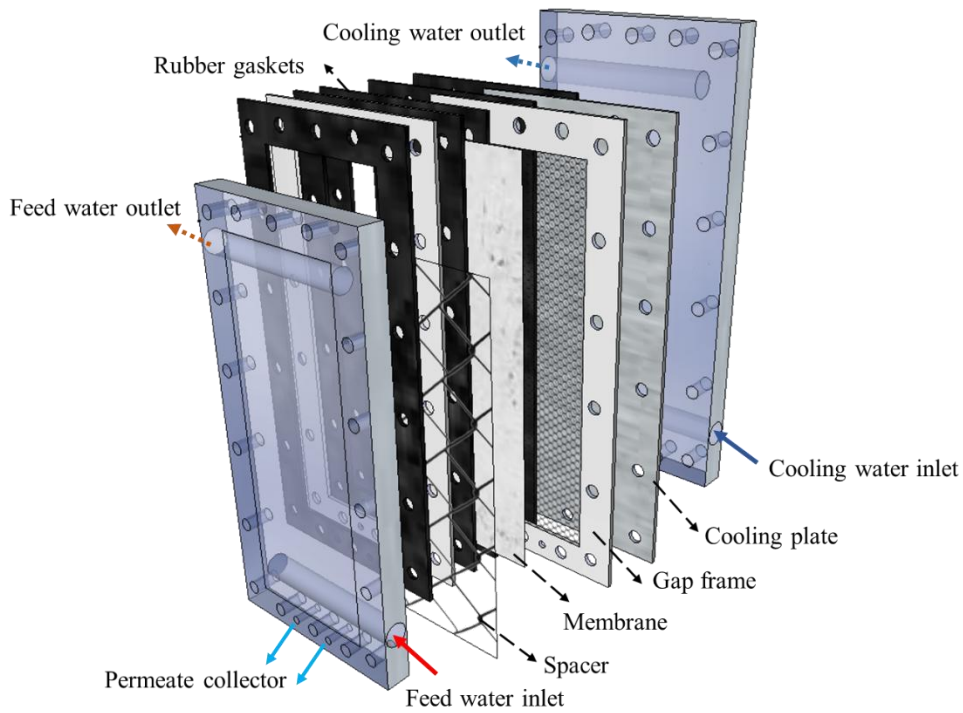
180

181 Further experiments were conducted to better understand the behavior of HA in AGMD, by
 182 implementing a double gap width (total thickness of 6 mm) into the module. In this case, feed
 183 water was slightly changed using deionized water and 50 mg L⁻¹ of HA to avoid saline
 184 interferences and a high HA concentration. This mode was compared to AGMD and WGMD
 185 keeping the same feed water and the experimental conditions.

186 Finally, Naidu et al (Naidu et al., 2015) reported thermal degradation of HA where lower
 187 molecular sized HS and other organics were observed. Hence, tests using a rotary evaporator
 188 (Tokyo Rikakikai SB-650 N-N, Japan) were carried out, recreating MD tests with seawater and
 189 synthetic water in order to determine if HA presence in the permeate was because of the MD
 190 process or to a greater volatility of HA thermal degradation byproducts.



191



192

193 **Fig. 1.** Schematic co-current AGMD/WGMD setup used in this work and MD module details.

194

195 *2.3. Analytical techniques*

196 The concentration of HA in the feed and permeate was measured mainly by total organic carbon

197 analyser (TOC-V CSH, Shimadzu, Kyoto, Japan), as suggest Meng et al (Meng et al., 2014).

198 NPOC method was used for all organic carbon measurements. Complementary measurements

199 using a UV spectrophotometer (UV-1800, Shimadzu, Kyoto, Japan) at the wavelength of 254
200 nm were used, according to Han and Myat et al (Han et al., 2017; Myat et al., 2012). Both
201 instruments were calibrated, resulting in a linear relationship in the HA concentration range of
202 0-100 mg L⁻¹, with a regression coefficient of 0.999 and 0.998, respectively. Furthermore,
203 fluorescence excitation-emission spectra (EEM) were recorded on a fluorescence
204 spectrophotometer (Horiba Scientific Aqualog, Kyoto, Japan). These spectra were compared
205 with previous studies related to HA and OM (Rodríguez et al., 2014; Wang et al., 2009).

206 Contact angle with deionized water and with HA solution was examined for each membrane,
207 using a Contact Angle Analyser (Kruss DSA25). An average of four measurements at different
208 locations of the membrane were taken by the static sessile drop method and the average value is
209 reported.

210 Finally, the various MD tests and sample measurements were carried out at least in triplicate, in
211 order to demonstrate the confidence of the results obtained. In addition, all results were verified
212 with calibration curves, as well as TOC and HA flow data were found above with LOD (0.30
213 mg L⁻¹) and LOQ (0.44 mg L⁻¹) in all cases.

214 3. Results and discussion

215 3.1. MD performance with real seawater and synthetic saline water with HA

216 Results for all experiments performed with both MD configurations and feed solutions are
217 shown in Table 2. In all cases, the saline rejection factor, RF_{EC} , (based on EC measurement) was
218 above 99%. This shows that membrane wetting has likely not taken place and membranes were
219 intact during the experiments. Meanwhile RF_{NPOC} showed lower values, reaching a minimum
220 value of 33 ± 11 % and no higher than 93% in all cases. Seawater tended to show lower RF_{NPOC}
221 values suggesting a different property of the organics. The carbon and representative HA flux
222 are shown in Table 3. However the lower rejection of organics compared to EC shows that even
223 for synthetic saline water, organic material is diffusing through the membrane. In the case of

224 synthetic water where the only organic material added was HA, it confirms that this diffusion is
 225 by HA molecules.

226 **Table 2.** Average permeate EC, NPOC, RF_{EC} and RF_{NPOC} for different MD configuration and
 227 feed water. Initial conditions for feed seawater: EC: $44057 \pm 1858 \mu\text{S cm}^{-1}$, NPOC: 2.6 ± 0.2
 228 mg L^{-1} . Initial conditions for feed synthetic water: EC: $3340 \pm 180 \mu\text{S cm}^{-1}$, NPOC: 16.3 ± 1.8
 229 mg L^{-1} . TOC LOD: 0.30 mg L^{-1} ; TOC LOQ: 0.44 mg L^{-1} .

		EC	NPOC	RF_{EC}	RF_{NPOC}
		$\mu\text{S cm}^{-1}$	mg L^{-1}	%	%
AGMD	Seawater	40 ± 21	1.7 ± 0.3	99.9 ± 0.1	33 ± 11
	Synthetic water	14 ± 1	1.7 ± 0.7	99.6 ± 0.0	90 ± 4
WGMD	Seawater	51 ± 20	0.8 ± 0.2	99.9 ± 0.0	68 ± 7
	Synthetic water	3 ± 0	1.2 ± 0.3	99.9 ± 0.0	93 ± 2

230

231 **Table 3.** Carbon and representative HA flux for MD test using real seawater and average
 232 results (all operating conditions) for MD test using synthetic saline water with HA. Feed and
 233 cooling temperatures for seawater: 70°C and 18°C , respectively. Steady state fluxes for
 234 seawater tests: $3.3 \pm 0.2 \text{ L h}^{-1} \text{ m}^{-2}$ for AGMD and $8.1 \pm 1.0 \text{ L h}^{-1} \text{ m}^{-2}$ for WGMD.

235

Mode	Seawater		Synthetic water	
	Carbon Flux $\text{mgC h}^{-1} \text{ m}^{-2}$	HA Flux $\text{mgHA h}^{-1} \text{ m}^{-2}$	Carbon Flux $\text{mgC h}^{-1} \text{ m}^{-2}$	HA Flux $\text{mgHA h}^{-1} \text{ m}^{-2}$
AGMD	5.9 ± 1.4	21.5 ± 5.4	6.0 ± 2.5	21.6 ± 9.7
WGMD	6.4 ± 1.0	19.7 ± 4.4	8.2 ± 2.7	27.9 ± 10.3

236

237 3.2. Rotary evaporator tests with real seawater and synthetic saline water with HA

238 Results obtained in the rotary evaporator tests are shown in Table 4. The experiments were
 239 carried out under the same conditions as in MD for convenient comparison. EC was measured
 240 in some permeate samples, where EC values below $3 \mu\text{S cm}^{-1}$ were obtained in all cases. The
 241 RF_{EC} therefore reached where $>99\%$ and compared well with the MD tests shown in Table 2.
 242 However a major difference was to NPOC rejection, where the distillate concentrations were
 243 very similar to the blank (deionized water) in all cases showing that HA compounds and OM
 244 contained in both synthetic water and seawater are not volatile. In addition, it is verified that HS

245 thermal degradation byproducts do not pass into the vapor phase. In this sense, HA diffusion
 246 process through the membrane is inherent to the MD process. Therefore the next part of this
 247 work will be to explore the effect of typical MD operating conditions on the diffusion of HA.

248 **Table 4.** NPOC values for seawater and synthetic water using rotary evaporator.

	Seawater			Synthetic water		
	Feed	Condensate	Blank	Feed	Condensate	Blank
NPOC mg L ⁻¹	2.6 ± 0.2	0.4 ± 0.2	0.4 ± 0.2	16.3 ± 1.8	0.6 ± 0.1	0.4 ± 0.1

249

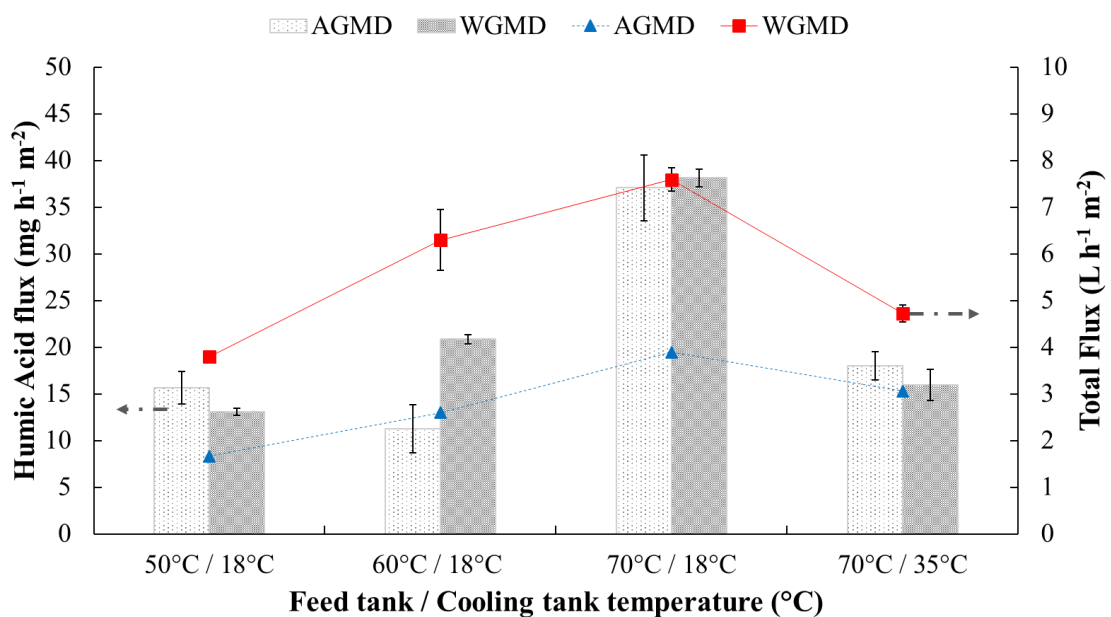
250 3.3. Effect of MD operating conditions on HA diffusion

251 3.3.1. Effect of operating temperatures

252 Fig.2 shows the influence of different operating temperatures on the HA flux through the
 253 membrane. As it can be seen, HA flux was increased (from 15.6 to 37.1 mg h⁻¹ m⁻² for AGMD
 254 and 13.1 to 38.1 mg h⁻¹ m⁻² for WGMD) with higher feed temperatures in the same manner as
 255 the total flux (from 1.7 to 3.9 L h⁻¹ m⁻² for AGMD and 3.8 to 7.6 L h⁻¹ m⁻² for WGMD).
 256 Nevertheless, when the cooling temperature set to 35°C keeping feed temperature at 70°C, total
 257 flux decreased (3.1 L h⁻¹ m⁻² and 4.7 L h⁻¹ m⁻² for AGMD and WGMD, respectively) since there
 258 was a lower vapor pressure across the membrane. Likewise, HA flux decreased to 18.0 mg h⁻¹
 259 m⁻² for AGMD and 16.0 mg h⁻¹ m⁻² for WGMD. Based on this result, it appears that HA flux
 260 generally follows total flux, supporting the concept that HA is entrained through the membrane
 261 with water following the model proposed by Meng et al (Meng et al., 2014). However it is not a
 262 direct correlation since there was little or no increase in HA flux from 50°C to 60°C, but a large
 263 increase occurred from 60°C to 70°C. Meanwhile water flux increase was proportionately
 264 similar at each temperature step (cases of 18°C permeate cycle temperatures). This is evidence
 265 that water and HA diffusion are not entirely connected which will be further explored later in
 266 this paper. Comparing the HA flux obtained for AGMD and WGMD, both MD configurations
 267 showed a similar behavior where it should be expected no non-volatile HA would be present at
 268 all in AGMD permeate. In this way, several types of condensation may occur in AGMD

269 systems as is suggested by Warsinger et al (Warsinger et al., 2018) and therefore, the presence
 270 of HA flux in AGMD suggests liquid contact between the membrane and condensing plate.
 271 Additionally, in Figure 2 a discrepancy of HA fluxes for AGMD and WGMD in the test at a
 272 temperature of 60°C is reported. This performance could be also attributed to liquid contact
 273 between membrane and condensing plate (water bridging) in AGMD. Thus, water bridging
 274 could be different as the flux is lower, but when more water flux occurs, the risk of bridging
 275 increases rapidly, potentially due to rapid coalescence of condensed water clusters. This is
 276 potentially a reason why it rose suddenly for AGMD when water flux is higher.

277 Looking more closely at the chemistry, pH is known to play an important role in the behavior
 278 and solubility of HA (Khayet et al., 2004). However no large differences in pH were observed
 279 in the experiments carried out using synthetic water. The pH on average for AGMD was $6.39 \pm$
 280 0.26 while for WGMD was 6.66 ± 0.21 . Feed pH was 6.81 ± 0.31 . According to the results
 281 obtained, it can be assumed that HA behavior is not attributed to pH changes between feed and
 282 permeate. In terms of EC rejection, AGMD was slightly less effective than WGMD but both
 283 were >99%. The salinity may also play a role in the HA diffusion, where future work could
 284 consider the effect of total dissolved solids concentration, including effects of other trace
 285 minerals including calcium and iron.



286

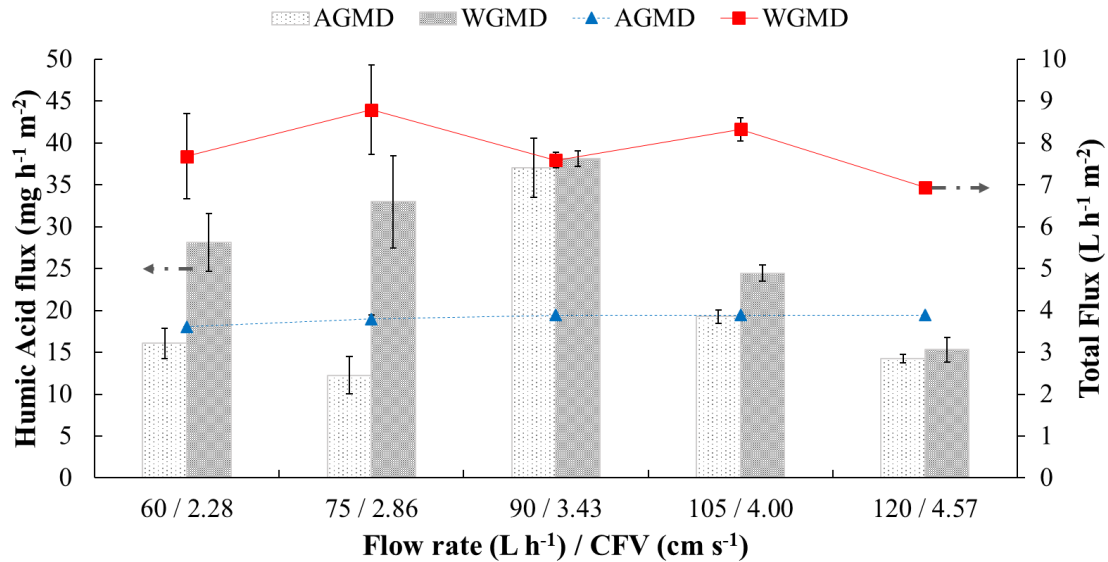
287 **Fig. 2.** HA flux obtained for PTFE membrane and both MD configurations at different operating
288 temperatures. Total flux is represented by lines graphed on the secondary axis. Feed and cooling
289 cycle flow rate: 90 L h⁻¹. Feed water: 1 g L⁻¹ NaCl, 0.88 g L⁻¹ CaCl₂ and 100 mg L⁻¹ HA. PTFE
290 membrane with effective area of 0.018 m². **Due to low errors on some points, error bars cannot**
291 **be seen.**

292

293 3.3.2. *Effect of cross flow rate*

294 Figure 3 shows the total flux and HA flux from MD testing on synthetic saline water with HA at
295 varied cross flows with fixed feed and permeate temperature conditions. AGMD total flux was
296 mostly constant (3.9 L m⁻² h⁻¹) for flow rates of 90, 105 and 120 L h⁻¹ but slightly increase by
297 7.75% over the entire range. WGMD showed large variations in total flux for flow rates of 60
298 and 75 L h⁻¹ but was generally higher than AGMD with flux values between (7 L m⁻² h⁻¹ and 9 L
299 m⁻² h⁻¹). **These total flux and HA flux variations in WGMD could be caused by the specific**
300 **operational features. For example, in WGMD, permeate is collected by overflow of the water**
301 **gap while AGMD is collected by gravity. Therefore, as a possible effect, WGMD permeate is**
302 **affected by the feed flow pushing on the membrane surface and in turn, membrane movement**
303 **generates a pulse effect in the gap. In this sense, flow rates greater than 75 L h⁻¹ generated a**
304 **constant total flux in all experiments. Nevertheless, for the studied flow rates of 60 L h⁻¹ and 75**
305 **L h⁻¹, the membrane pulse was lower, and consequently, total flux was more variable over time.**
306 In any case, errors in WGMD did not show a discernible trend, and the total flux overall trend
307 for both MD configurations indicated a low sensitivity of the total flux to CFV within the range
308 studied. However, considering this more carefully, temperature must also be considered with
309 varying cross flow as it is a key factor for MD process. In all cases, high EC rejections were
310 obtained (99.9% for WGMD and 99.6% for AGMD) and pH values (6.5 and 6.4 for WGMD
311 and AGMD, respectively) were similar and comparable to temperature tests. **In the studied**
312 **range, a change in flow rates keeping temperatures constant does not significantly affect the**
313 **vapor pressure difference across the membrane and consequently, total fluxes are almost**
314 **constant.** This does not mean that in other flow rate conditions, the reduced polarization effects
315 and a higher temperature profile uniformity, added to a thermal energy increase by higher **CFV,**
316 **would in turn substantially increase the total flux.**

317 Looking at HA fluxes the behavior was independent to that of total flux and showed a unique
 318 effect. Therefore, it has been further shown that HA can diffuse independently of water, where
 319 effects of cross flow will impact its diffusion. The functional effect cross flow has on HA
 320 diffusion may be its effect on the fluid-membrane interface (i.e. boundary layer).

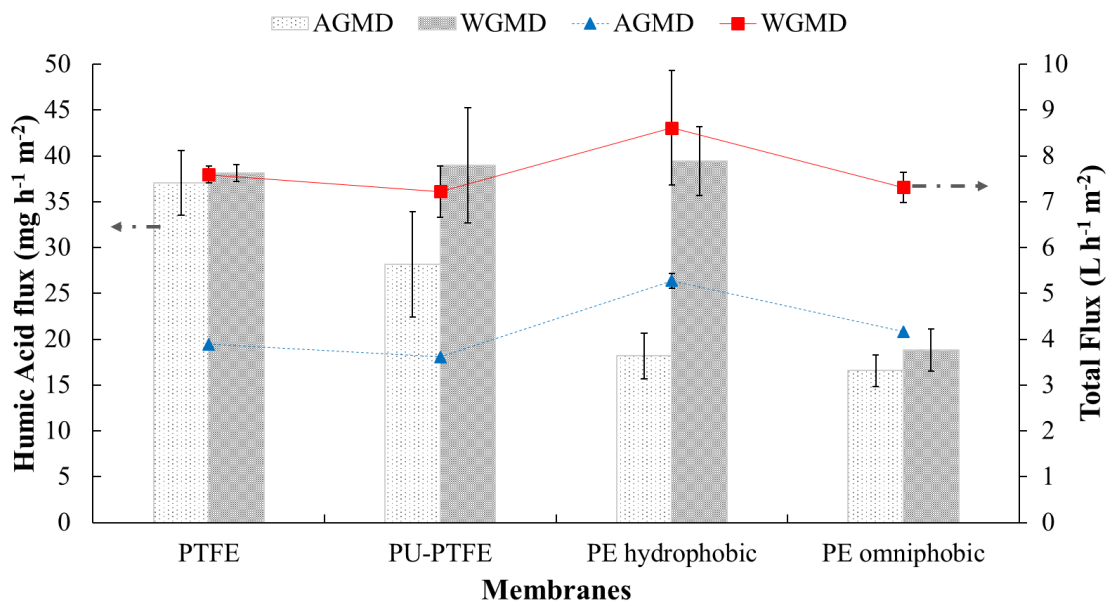


321
 322 **Fig. 3.** HA flux obtained for PTFE membrane and both MD configurations at different flow
 323 rates and CFV. Total flux is represented by lines graph on a secondary axis. Feed and cooling
 324 temperatures: 70°C and 18°C, respectively. Feed water: 1 g L⁻¹ NaCl, 0.88 g L⁻¹ CaCl₂ and 100
 325 mg L⁻¹ HA. PTFE membrane with effective area of 0.018 m². Due to low errors on some points,
 326 error bars cannot be seen.

327
 328 In these tests, HA flux showed a clear trend. At lower CFVs, 2.28 and 2.86 cm s⁻¹, HA flux for
 329 AGMD showed low values. The explanation could be related to a higher mass transfer
 330 resistance of the AGMD, as will be discussed in section 3.4. However, it peaks considerably at
 331 the middle range CFV at 3.43 cm s⁻¹. Meanwhile, HA flux for WGMD showed a similar peak at
 332 this CFV but gave higher initial values at the lower CFVs tested. For higher CFVs to 3.43 cm s⁻¹,
 333 a clearly descending trend can be observed for HA flux in both MD configurations, reaching a
 334 minimum HA flux by WGMD at CFV of 4.57 cm s⁻¹. A mechanisms of HA diffusion related to
 335 the flow across the membrane surface has become evident, which will be discussed later. The
 336 next section will consider the membrane surface chemistry to further explore the effect of the
 337 liquid-membrane surface interactions on HA flux.

338 3.3.3. Effect of membrane chemistry

339 Fig.4 shows the results for tests on the standard hydrophobic PTFE membrane compared to
 340 other membrane types to explore the influence of different materials on the HA flux in
 341 permeate. PU-PTFE (hydrophilic PU coated hydrophobic PTFE), hydrophobic PE and
 342 omniphobic PE showed similar results to the standard PTFE membranes in terms of total flux.
 343 EC rejection (99.6% AGMD and 99.9% for WGMD) and pH of AGMD and WGMD permeates
 344 (6.4 and 6.5, respectively) were similar in all cases and behavior similar to both temperature and
 345 flow rate cases. However difference were observed between the membrane chemistries for HA
 346 flux. HA flux through the PTFE membrane is highest in both AGMD and WGMD, and similar
 347 to PU-PTFE within error. Meanwhile PE hydrophobic was only similar in HA flux for WGMD
 348 mode, while AGMD mode showed HA flux was about 50% of any of these higher values. This
 349 small value was similar for PE omniphobic, uniquely in both AGMD and WGMD.



350

351 **Fig. 4.** HA flux obtained for different membranes and both MD configurations. Total flux is
 352 represented by lines graph on a secondary axis. Feed and cooling temperatures: 70°C and 18°C,
 353 respectively. Feed and cooling cycle flow rate: 90 L h⁻¹. Feed water: 1 g L⁻¹ NaCl, 0.88 g L⁻¹
 354 CaCl₂ and 100 mg L⁻¹ HA. Each membrane has an effective area of 0.018 m². Due to low errors
 355 on some points, error bars cannot be seen.

356 In relation with other membranes tested, omniphobic PE membrane with about 50% of the HA
 357 flux through PTFE in both AGMD and WGMD while at the same time as maintaining a similar

358 level of total flux. Clearly membrane chemistry is influencing the HA flux, where a
359 hydrophobic chemistry favours HA diffusion in the liquid-liquid feed-permeate contact WGMD
360 mode. This is also true for PU-PTFE where despite the hydrophilic PU coating facing the feed
361 solution, HA still diffused into the permeate through the underlying hydrophobic PTFE layer.
362 The omniphobic membrane possessed also the ability to repel hydrophobic interactions
363 indicating the HA diffusion through MD membranes is due to hydrophobic interactions between
364 the membrane and the HA molecule. The outstanding result was for the hydrophobic PE
365 membrane which gave HA fluxes for WGMD similar to the PTFE membranes, but gave lower
366 HA flux in AGMD similar to the omniphobic PE membrane. This result cannot be fully
367 explained based on the present data, and may be due to differences in the hydrophobicity of the
368 PE material compared to PTFE that yielded differences between the MD modes where AGMD
369 may have had less water bridging and in turn reduced HA flux.

370 Contact angle (CA) was measured on virgin membranes using synthetic water (1 g L⁻¹ NaCl,
371 0.88 g L⁻¹ CaCl₂ and 100 mg L⁻¹ HA) and deionized water measurement in order to confirm the
372 hydrophobicity of the membrane surfaces. A MD membrane with a water contact angle above
373 90° is considered hydrophobic (García-Fernández et al., 2015). In this way, according to water
374 CA measured, PTFE (97°) and both PE membranes (106° for hydrophobic and 122° for
375 omniphobic) exhibited hydrophobic surfaces, while hydrophilic PU-PTFE membrane showed a
376 water CA around 69° showing a hydrophilic surface, due to the PU coating on the underlying
377 hydrophobic PTFE that blocks liquid water.

378 Furthermore, CA measurements using synthetic water supported the same theory explained
379 previously using deionized water. In this way, synthetic water CA measured for each membrane
380 was 88° for PTFE, 72° for PTFE-PU, 114° for PE hydrophobic and 127° for PE omniphobic.
381 Although HA interaction with the membrane surface cannot be completely explained only by
382 the CA analysis, a trend is observed among the CA and the HA flux using synthetic water, even
383 for the PTFE-PU membrane, which is a composite membrane where only its surface facing the
384 liquid is hydrophilic.

385 In this sense, it is important to highlight the CA analysis to omniphobic PE membrane, which
386 presents the lowest values of HA flux and, in turn, the highest CA values (122° and 127° for
387 deionized water and synthetic water, respectively). These results suggest that modified
388 membranes could play an important role in OM rejection and other elements with the same
389 features. Meanwhile, the unusual result for the hydrophobic PE membrane in Figure 4 observed
390 earlier may be explained by the relatively higher CA. When the gap is filled with water in the
391 case of WGMD, HA may freely diffuse from the membrane surface into the permeate liquid. On
392 the other hand, for AGMD the more hydrophobic surface could have assisted in repelling the
393 bridging of liquid water from the permeate membrane surface across the gap to the condensing
394 plate sufficiently more than both PTFE membranes. The more intact air gap therefore acted as a
395 barrier to HA flux being more like the rotary evaporator test where HA could not be entrained
396 into the distillate through the vapour phase. Furthermore, the study of other membrane
397 properties such as thickness, porosity and tortuosity would play a role, so a detailed analysis of
398 such properties on these membranes is needed to extend our current study to explore means to
399 understand and control HA diffusion through MD membranes.

400 In conclusion, even though there are no large changes in the total flux, a clear decrease in the
401 HA flux was obtained for omniphobic PE membrane and for the high CA hydrophobic
402 membrane in AGMD mode. Therefore, according with works from other authors (Damtie et al.,
403 2018; Duong et al., 2018; Wang et al., 2018; Woo et al., 2016; Zheng et al., 2018) and the
404 results obtained in this study, we conclude that MD membranes play an important role in the
405 quality of the permeated water.

406 *3.4. HA diffusion models*

407 According to results obtained for MD tests using synthetic water, HA diffusion models can now
408 be proposed based on the key operating conditions of temperature and flow rate.

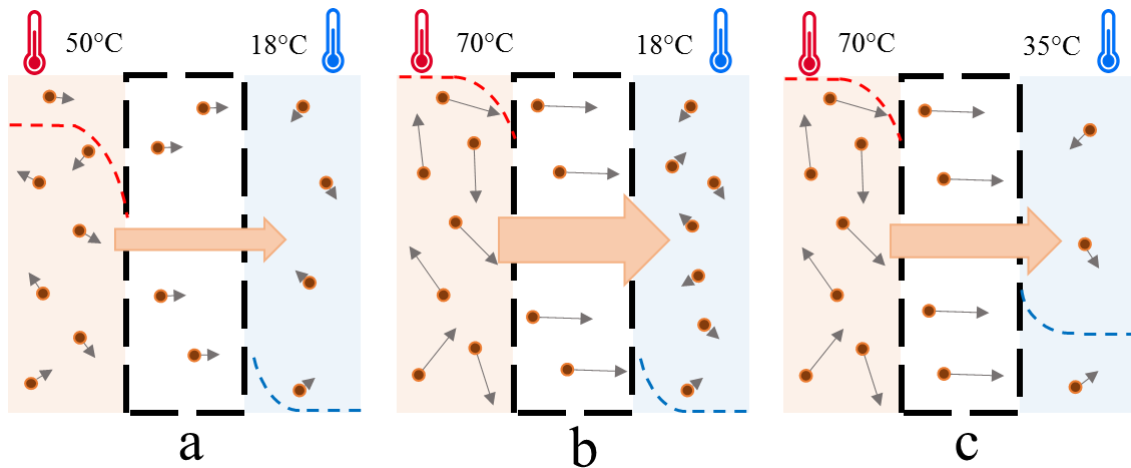
409 Experimental data suggest that the HA diffusion as a function of temperature can be explained
410 by Fick's Law. Thus, the diffusivity of HA within the membrane and the HA driving force

411 across the membrane surfaces are the main phenomena that could affect the flux. Hence, it is
412 observed that the increase in feed temperature increased the HA flux and therefore, the
413 temperature influences the HA diffusivity. However, the increase in permeate temperature
414 showed a considerable decrease in HA flux, so it seems to be strongly related to the HA driving
415 force based on the surface concentrations of HA. Taking the latter into account as well as the
416 results obtained for flux and membranes tests, it is suggested that the increase in feed
417 temperature raised the concentration of HA on the membrane surface by increasing its access
418 from the bulk to the surface, potentially from increased diffusion through the boundary layer.
419 So, when permeate temperature increased, total flux decreased and the concentration
420 polarization of HA from water flux on the feed declined. Figure 5 shows the proposed model for
421 the HA diffusion because of temperature.

422 **In addition**, another phenomenon could affect in a complementary way to overall HA flux, by
423 which, the adsorption of HA on the surface of the membrane decreases with the increase in
424 temperature, while the diffusivity of HA increases.

425 **In this sense, the discrepancy obtained for the HA flux in AGMD at 60°C (Figure 2) could be**
426 **explained both to the effect of the water bridges, to the diffusion models, discussed above, and**
427 **to small structural changes of the HA with temperature. In the latter case, some authors**
428 **(Giovanela et al., 2010, 2004; Kolokassidou et al., 2007) reported that there are small changes**
429 **in the structure of HA resulting in a loss of mass in the temperature range of 40°C to 80°C.**
430 **These changes are related to the reversible and irreversible losses of different types of water**
431 **molecules contained in the HA. Thus, reversible structural changes occur at around 60°C, while**
432 **irreversible changes become important at 70°C (formation of more condensed and hydrophobic**
433 **polyaromatic structures) (Giovanela et al., 2010, 2004; Kolokassidou et al., 2007). Based on**
434 **these studies, in MD tests at temperatures of 60°C, it is suggested that HA molecules loaded**
435 **with water coexist with HA molecules with more condensed reversible structures. Therefore,**
436 **while for WGMD both types of molecules could be diffused without high resistance to**
437 **permeate, the heavier HA molecules would have lower diffusion because of the higher mass**

438 transfer resistance of AGMD due to the air gap (Alkudhiri et al., 2012a). In addition, the effect
 439 of less water bridges in AGMD at lower fluxes (section 3.3.1) could be considerable. For these
 440 reasons, the HA flux in the AGMD is lower than the WGMD under these experimental
 441 conditions. However, there is not enough evidence to conclude if the sudden rise in HA flux at
 442 70°C is due to altered HA chemistry or an accelerated water bridging effect.

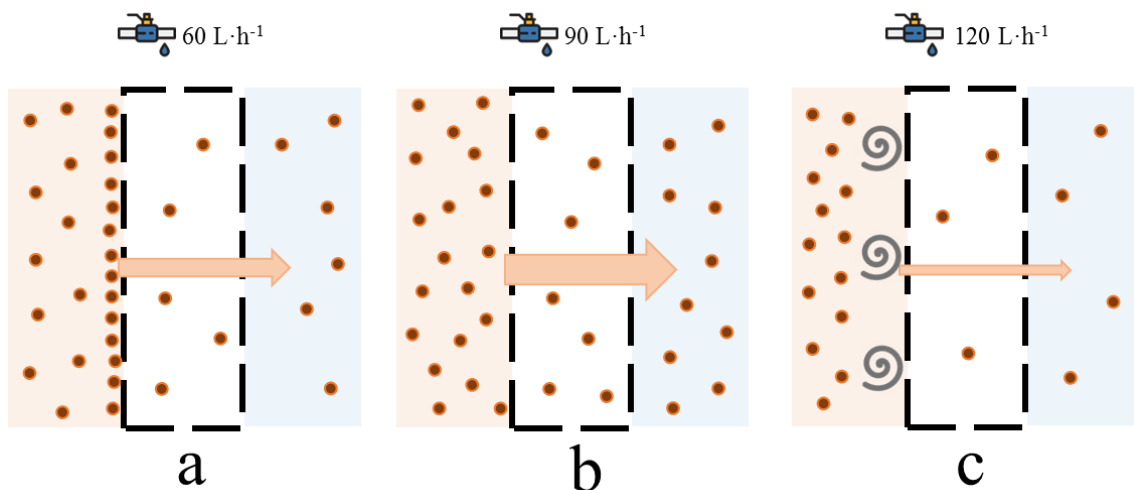


443 **Fig. 5.** HA diffusion in AGMD and WGMD because of temperature. Low temperatures imply a
 444 low particle speed and therefore, less diffusivity through the boundary layer (a). Higher
 445 temperatures assisted HA flux by improving diffusion of accumulated HA at the membrane
 446 surface (b). Permeate side temperature increase implies a HA concentration polarization
 447 decrease (c).
 448

449
 450 HA flux trend for flow rates tests can be explained by three different process as is illustrated in
 451 Fig.6. Firstly, at lower flow rate and cross flow velocity (2.28 cm s^{-1}), concentration polarization
 452 and boundary layer phenomena are significant leading to high HA concentration at the surface
 453 under relatively quiescent conditions. In this way, most of molecules and colloids of HA were
 454 deposited on the membrane surface, inhibiting HA diffusion through the membrane. For
 455 AGMD, at lower CFV (2.28 and 2.86 cm s^{-1}), lower HA flux compared to WGMD was
 456 obtained, as it was shown in Figure 3. These results suggested a CFV influence by concentration
 457 polarization and boundary layer phenomena. Thus, at low CFV, the residence time of HA on the
 458 membrane surface is longer. Therefore, with low velocity, higher concentration polarization, as
 459 well as a higher AGMD resistance to mass transfer, this resulted in a lower HA diffusion in this

460 MD configuration. Nevertheless, in WGMD, as a result of lower mass resistance, the HA
461 diffuses more easily to permeate under the same experimental conditions.

462 As the flow and CFV increased, the feed water mixture was increasingly homogeneous. For this
463 reason, the concentration polarization and associated boundary layer and HA fouling layer
464 phenomena were weakened, and HA diffusion to permeate reached a maximum at 90 L h⁻¹.
465 From this point, although the mixture is homogeneous at higher flow rates, HA flux dropped
466 noticeably at CFV of 4.00 and 4.57 cm s⁻¹. The latter process suggests the influence of shear
467 forces, which complicate HA transport to the membrane surface. It appears some accumulation
468 within the boundary layer is needed for HA flux to occur. With too much mixing and the
469 surface condition approaching the bulk solution, HA flux becomes reduced.



470
471 **Fig. 6.** Influence of the flow rates in HA diffusion for AGMD and WGMD. Predominance of
472 boundary layer phenomena and concentration by polarization (a). Complete mixture of feed
473 cycle, reaching the maximum diffusion (b). Shear forces play an important role at higher
474 flow rates (c).

475
476 To date, only a few studies have detected HA in permeate and their migration through the
477 membrane in DCMD. According to Meng et al (Meng et al., 2014), the process involves HA
478 adsorption-desorption onto the membrane surface, because of amphiphilic nature of HA. Thus,
479 HA migrates through the membrane pores by hydrogen bonding between water vapor and
480 humic molecules. This process suggests a dependence between migration mechanism and vapor
481 pressure and therefore, with the total flux for DCMD.

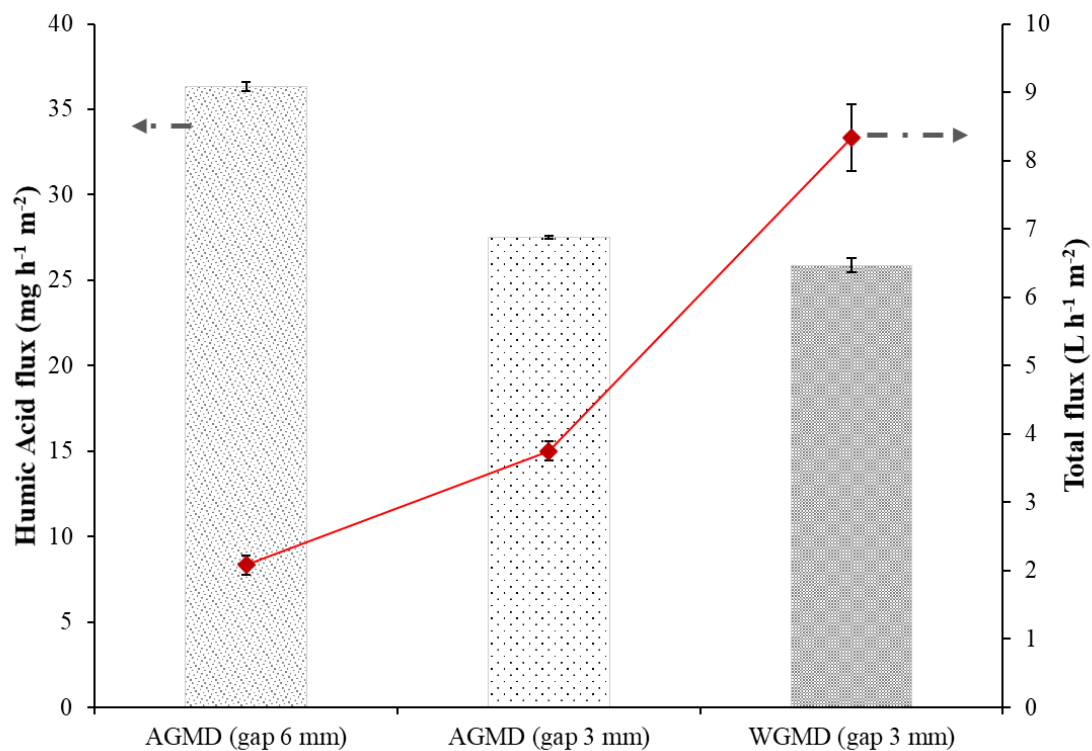
482 According to the results obtained for all tests carried out in this work and diffusion models
483 suggested, HA behavior based on diffusion is proposed for AGMD and WGMD. The diffusion
484 mechanism is independent of total flux and consequently, vapor pressure as well. AGMD and
485 WGMD have been used with the purpose of analyzing an isolated permeate, avoiding the
486 dilution effect in DCMD and therefore, not underestimating the amount of HA or NOM present
487 in permeate.

488 *3.5. Complementary studies*

489 *3.5.1. Double gap width for AGMD*

490 Following our finding earlier where HA flux occurred in AGMD as well as WGMD, water
491 bridges have been proposed by which HA could diffuse into permeate. These water bridges can
492 play an important role in this phenomenon, because of an additional sweeping effect of the
493 membrane cold side (Warsinger et al., 2018).

494 In relation to this suggestion, an additional frame was installed in order to double the gap size to
495 6 mm. Thus, a significant decrease in both total and HA fluxes could be expected. In this regard,
496 as it can be seen in Fig.7, while the total flux dropped noticeably, the HA flux detected was
497 greater (around 36%) than that obtained for 3 mm gap. Although a wider gap implied less water
498 bridging as well as total flux drop, slightly increased HA flux was obtained. These results
499 suggest that HA flux is not relying on total flux, and HA diffuses through the membrane in any
500 case. In addition, HA flux increase may be due to new conditions for wider gap as for example,
501 a favorable change in the temperature profile for HA diffusion. For example, at lower fluxes,
502 temperature polarization will be lower leading to larger temperature differences over the
503 membrane. As concluded earlier, the higher temperature on the feed side assisted HA flux by
504 improving its ability to diffuse through boundary layers containing accumulated HA at the
505 membrane surface which could also be eliminated by increasing cross flow (but only up to a
506 certain point).



507

508 **Fig. 7.** HA flux obtained for different gap tests. Total flux is represented by the lines with the
 509 values indicated on the secondary axis. Feed and cooling temperatures: 70°C and 18°C,
 510 respectively. Feed and cooling cycle flow rate: 90 L h⁻¹. Feed water: Deionized water and 50 mg
 511 L⁻¹ HA to avoid influence of salts and high HA concentrations. PTFE membrane with an
 512 effective area of 0.018 m². **Due to low errors on some points, error bars cannot be seen.**

513

514 3.5.2. HA preliminary characterization

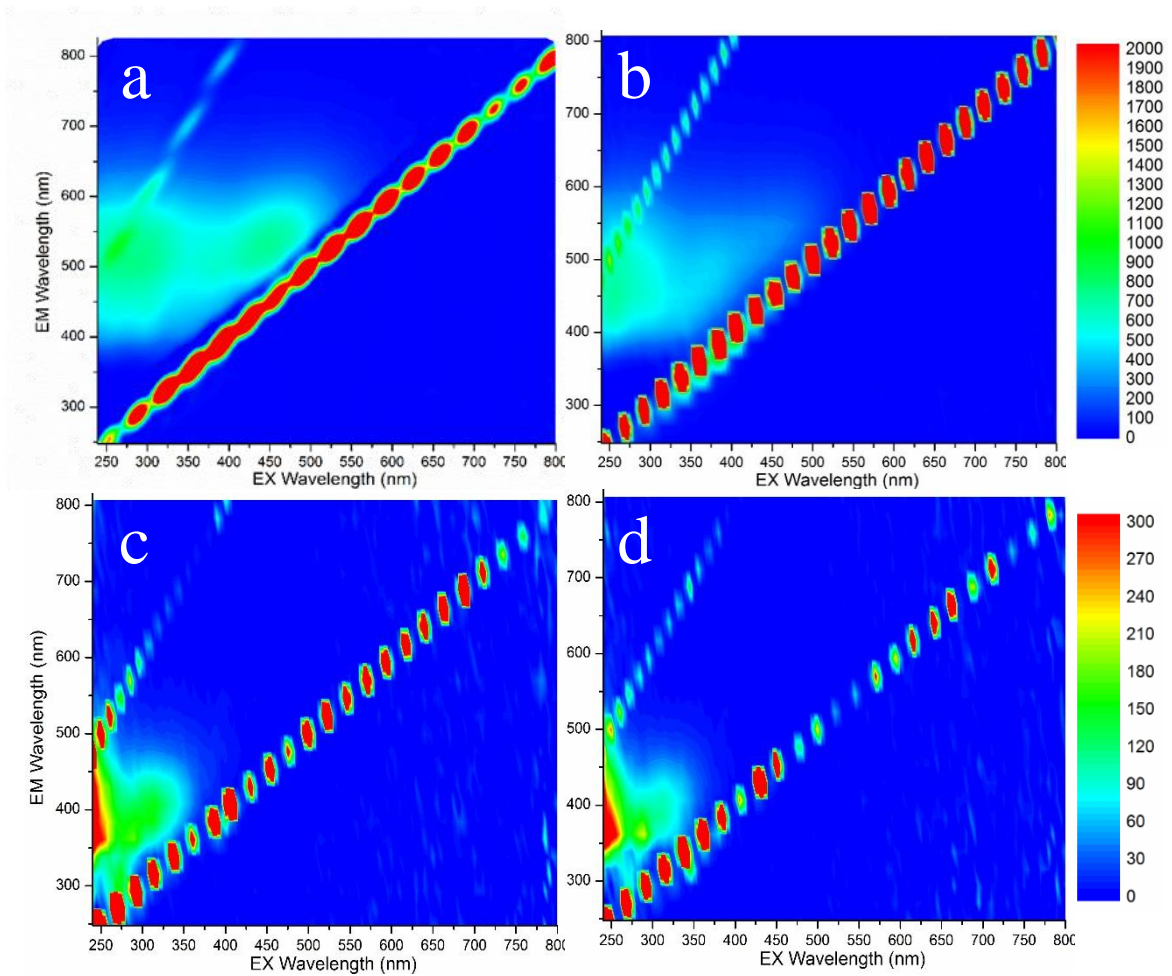
515 Using appropriate calibration curves for UV spectrometer and TOC analyzer, a good correlation
 516 was achieved for the synthetic water. This means that the absorbance could be known from the
 517 NPOC value and, therefore, the concentration of HA in the sample, indistinctly. Errors using the
 518 correlation between both techniques were less than 10%, with an average value of 7%. It is
 519 important to underline that different high and low range HA calibration curves were applied in
 520 order to cover the entire range of concentrations.

521 On the contrary, when these correlation equations were applied for UV spectrophotometer and
 522 TOC analyzer in permeate samples, errors obtained were above 87%. In addition, the
 523 absorbance values obtained in the permeate samples did not correspond to the absorbance that
 524 would have a feed water with the same concentration of HA measured with TOC analyzer. For

525 these reasons, a profile change in the HA molecule is suggested, since it seems that the HS
526 found in permeate absorb UV differently and therefore, they have different properties to the
527 original HS contained in the feed water.

528 The composition differences of HA in feed and permeate was also analyzed using fluorescence
529 spectrophotometry. Nevertheless, Excitation – Emission Matrix (EEM) fluorescence spectra can
530 be altered by pH and salt concentrations in the sample. In order to study the possible saline
531 interferences and differences between feed and permeate EEM spectra (Fig.8), fluorescence
532 measurements were made using different concentrations of HA in deionized water without salts,
533 as well as synthetic water (MD feed water) at different concentrations of HA. In all these
534 measurements, EEM spectra similar to each other were obtained. In Fig. 8a an EEM spectrum of
535 HA in deionized water (without added salts) is shown.

536 In Fig.8.b, an EEM fluorescence spectrum obtained from a synthetic water feed sample is
537 shown. This spectrum presents typical values for a standard HA, showing two Ex/Em peaks
538 around 250-350/450 nm (Rodríguez et al., 2014). High similarities between the EEM spectra of
539 synthetic water feed and HA with deionized water are observed. Both EEM spectra showed the
540 same profile as well as the peaks related to HA. Additionally, EEM spectra for AGMD and
541 WGMD permeate samples are shown in Fig. 8c and 8d, respectively. The spectra obtained for
542 the permeate samples in both MD configurations are very similar to each other, showing a
543 maximum Ex/Em peak around 250/350-400 nm. Although these permeate EEM spectra showed
544 fluorescence characteristics corresponding to humic acid-like substances (Wang et al., 2009),
545 clear differences in relation to the feed EEM spectrum and also, with HA in deionized water
546 EEM spectrum were observed. These results suggest and confirm a change in the HA profile
547 diffused through the membrane, as was previously proposed with the UV spectrometer
548 measurements.



549

550 **Fig. 8. a.** EEM spectrum for HA in deionized water; **b.** EEM spectrum for synthetic feed water
 551 sample; **c.** EEM spectrum for AGMD permeate sample; **d.** EEM spectrum for WGMD permeate
 552 sample.

553

554 **4. Conclusions**

555 Tests with different operating temperatures, flow rates and MD membranes were performed in
 556 order to study HA behavior, using AGMD and WGMD configurations. Non-volatile compounds
 557 have been detected in permeate, and humic flux through the membrane was affected by feed and
 558 cooling temperatures, boundary layers phenomenon, polarization concentration and shear
 559 forces. In addition, omniphobic PE membrane showed better HA rejection than the other
 560 membranes tested. In this way, MD membrane could play an important role in MD, which
 561 suggests that MD membrane is not only a passive element in the process. The same HA or

562 NOM behavior was obtained using both seawater and synthetic water. Therefore, a HA and
563 NOM diffusion mechanism is proposed for AGMD and WGMD configurations.

564 On the other hand, a sweeping effect on the membrane cold side was detected in AGMD
565 because of the frame, which separates the membrane and the cooling plate, acts as an
566 intermediate condenser. Humic flux in AGMD could be similar as in WGMD because of this
567 sweeping effect of the membrane.

568 Finally, a preliminary characterization of HA in MD permeate was carried out. HA differences
569 in permeate and feed were detected. In this way, it is necessary to go in depth with HA
570 characterization of MD permeate in order to analyze the OM complexation capacity and the
571 transport of undesired compounds through the membrane.

572

573 **Acknowledgments**

574 Authors want to acknowledge to University of Cadiz for supporting a predoctoral contract
575 within the Researcher Personnel Training Program (ref. 2015-036/PU/EPIF-FPI-CT/CP).

576 Leslie Naidoo of Australian Textile Mills is acknowledged for providing the laminated PU-
577 PTFE membranes used in this study.

578 Bart Nelemans of Aquastill is acknowledged for providing the hydrophobic PE and oleophobic
579 PE membranes used in this study.

580

581 **References**

582 Alkhudhiri, A., Darwish, N., Hilal, N., 2012a. Membrane distillation: A comprehensive review.
583 Desalination 287, 2–18. <https://doi.org/10.1016/j.desal.2011.08.027>

584 Alkhudhiri, A., Darwish, N., Hilal, N., 2012b. Treatment of high salinity solutions: Application
585 of air gap membrane distillation. Desalination 287, 55–60.

586 <https://doi.org/10.1016/j.desal.2011.08.056>

587 Alkhudhiri, A., Hilal, N., 2017. Air gap membrane distillation: A detailed study of high saline
588 solution. *Desalination* 403, 179–186. <https://doi.org/10.1016/j.desal.2016.07.046>

589 Amaya-Vías, D., Nebot, E., López-Ramírez, J.A., 2018. Comparative studies of different
590 membrane distillation configurations and membranes for potential use on board cruise
591 vessels. *Desalination* 429, 44–51. <https://doi.org/10.1016/J.DESAL.2017.12.008>

592 Anand, A., Unnikrishnan, B., Mao, J.Y., Lin, H.J., Huang, C.C., 2018. Graphene-based
593 nanofiltration membranes for improving salt rejection, water flux and antifouling—A
594 review. *Desalination* 429, 119–133. <https://doi.org/10.1016/j.desal.2017.12.012>

595 Attia, H., Alexander, S., Wright, C.J., Hilal, N., 2017a. Superhydrophobic electrospun
596 membrane for heavy metals removal by air gap membrane distillation (AGMD).
597 *Desalination* 420, 318–329. <https://doi.org/10.1016/j.desal.2017.07.022>

598 Attia, H., Osman, M.S., Johnson, D.J., Wright, C., Hilal, N., 2017b. Modelling of air gap
599 membrane distillation and its application in heavy metals removal. *Desalination* 424, 27–
600 36. <https://doi.org/10.1016/j.desal.2017.09.027>

601 Biel-Maeso, M., Baena-Nogueras, R.M., Corada-Fernández, C., Lara-Martín, P.A., 2018.
602 Occurrence, distribution and environmental risk of pharmaceutically active compounds
603 (PhACs) in coastal and ocean waters from the Gulf of Cadiz (SW Spain). *Sci. Total*
604 *Environ.* 612, 649–659. <https://doi.org/10.1016/J.SCITOTENV.2017.08.279>

605 Bond, T., Goslan, E.H., Parsons, S.A., Jefferson, B., 2012. A critical review of trihalomethane
606 and haloacetic acid formation from natural organic matter surrogates. *Environ. Technol.*
607 *Rev.* 1, 93–113. <https://doi.org/10.1080/09593330.2012.705895>

608 Chowdhury, S., Khan, N., Kim, G.-H., Harris, J., Longhurst, P., Bolan, N.S., 2016. Zeolite for
609 Nutrient Stripping From Farm Effluents, in: *Environmental Materials and Waste*. Elsevier,
610 pp. 569–589. <https://doi.org/10.1016/B978-0-12-803837-6.00022-6>

- 611 Criscuoli, A., Carnevale, M.C., 2015. Desalination by vacuum membrane distillation: The role
612 of cleaning on the permeate conductivity. *Desalination* 365, 213–219.
613 <https://doi.org/10.1016/J.DESAL.2015.03.003>
- 614 Cui, Z., Zhang, Y., Li, X., Wang, X., Wang, Z., Zhao, S., 2018. Optimization of novel
615 composite membranes for water and mineral recovery by vacuum membrane distillation.
616 *Desalination* 440, 39–47. <https://doi.org/10.1016/J.DESAL.2017.11.040>
- 617 Dantie, M.M., Kim, B., Woo, Y.C., Choi, J.-S., 2018. Membrane distillation for industrial
618 wastewater treatment: Studying the effects of membrane parameters on the wetting
619 performance. *Chemosphere* 206, 793–801.
620 <https://doi.org/10.1016/J.CHEMOSPHERE.2018.05.070>
- 621 Dow, N., Gray, S., Li, J. de, Zhang, J., Ostarcevic, E., Liubinas, A., Atherton, P., Roeszler, G.,
622 Gibbs, A., Duke, M., 2016. Pilot trial of membrane distillation driven by low grade waste
623 heat: Membrane fouling and energy assessment. *Desalination* 391, 30–42.
624 <https://doi.org/10.1016/j.desal.2016.01.023>
- 625 Duong, H.C., Chuai, D., Woo, Y.C., Shon, H.K., Nghiem, L.D., Sencadas, V., 2018. A novel
626 electrospun, hydrophobic, and elastomeric styrene-butadiene-styrene membrane for
627 membrane distillation applications. *J. Memb. Sci.* 549, 420–427.
628 <https://doi.org/10.1016/J.MEMSCI.2017.12.024>
- 629 Duong, H.C., Duke, M., Gray, S., Cooper, P., Nghiem, L.D., 2016. Membrane scaling and
630 prevention techniques during seawater desalination by air gap membrane distillation.
631 *Desalination* 397, 92–100. <https://doi.org/10.1016/j.desal.2016.06.025>
- 632 Essalhi, M., Khayet, M., 2015. Fundamentals of membrane distillation, in: *Pervaporation,*
633 *Vapour Permeation and Membrane Distillation.* Elsevier, pp. 277–316.
634 <https://doi.org/10.1016/B978-1-78242-246-4.00010-6>
- 635 Francis, L., Ghaffour, N., Alsaadi, A.A., Amy, G.L., 2013. Material gap membrane distillation:

636 A new design for water vapor flux enhancement. *J. Memb. Sci.* 448, 240–247.
637 <https://doi.org/10.1016/j.memsci.2013.08.013>

638 García-Fernández, L., Khayet, M., García-Payo, M.C., 2015. Membranes used in membrane
639 distillation: Preparation and characterization, Pervaporation, Vapour Permeation and
640 Membrane Distillation: Principles and Applications. [https://doi.org/10.1016/B978-1-](https://doi.org/10.1016/B978-1-78242-246-4.00011-8)
641 [78242-246-4.00011-8](https://doi.org/10.1016/B978-1-78242-246-4.00011-8)

642 Ghaffour, N., Missimer, T.M., Amy, G.L., 2013. Technical review and evaluation of the
643 economics of water desalination: Current and future challenges for better water supply
644 sustainability. *Desalination* 309, 197–207. <https://doi.org/10.1016/J.DESAL.2012.10.015>

645 Giovanela, M., Crespo, J.S., Antunes, M., Adamatti, D.S., Fernandes, A.N., Barison, A., da
646 Silva, C.W.P., Guégan, R., Motelica-Heino, M., Sierra, M.M.D., 2010. Chemical and
647 spectroscopic characterization of humic acids extracted from the bottom sediments of a
648 Brazilian subtropical microbasin. *J. Mol. Struct.* 981, 111–119.
649 <https://doi.org/10.1016/J.MOLSTRUC.2010.07.038>

650 Giovanela, M., Parlanti, E., Soriano-Sierra, E.J., Soldi, M.S., Sierra, M.M.D., 2004. Elemental
651 compositions, FT-IR spectra and thermal behavior of sedimentary fulvic and humic acids
652 from aquatic and terrestrial environments, *Geochemical Journal*.

653 González, D., Amigo, J., Suárez, F., 2017. Membrane distillation : Perspectives for sustainable
654 and improved desalination. *Renew. Sustain. Energy Rev.* 80, 238–259.
655 <https://doi.org/10.1016/j.rser.2017.05.078>

656 Guillen-Burrieza, E., Ruiz-Aguirre, A., Zaragoza, G., Arafat, H.A., 2014. Membrane fouling
657 and cleaning in long term plant-scale membrane distillation operations. *J. Memb. Sci.* 468,
658 360–372. <https://doi.org/10.1016/j.memsci.2014.05.064>

659 Han, L., Xiao, T., Zen, Y., Fane, A.G., Wei, J., 2017. Contaminant rejection in the presence of
660 humic acid by membrane distillation for surface water treatment. *J. Memb. Sci.* 541, 291–

661 299. <https://doi.org/10.1016/j.memsci.2017.07.013>

662 Herce-Sesa, B., López-López, J.A., Moreno, C., 2018. Multi-elemental ionic liquid-based
663 solvent bar micro-extraction of priority and emerging trace metallic pollutants (Cd, Ag,
664 Pd) in natural waters. *J. Hazard. Mater.* <https://doi.org/10.1016/J.JHAZMAT.2018.02.024>

665 Jermann, D., Pronk, W., Meylan, S., Boller, M., 2007. Interplay of different NOM fouling
666 mechanisms during ultrafiltration for drinking water production. *Water Res.* 41, 1713–
667 1722. <https://doi.org/10.1016/J.WATRES.2006.12.030>

668 Khalifa, A.E., 2015. Water and air gap membrane distillation for water desalination - An
669 experimental comparative study. *Sep. Purif. Technol.* 141, 276–284.
670 <https://doi.org/10.1016/j.seppur.2014.12.007>

671 Khalifa, A.E., Alawad, S.M., 2018. Air gap and water gap multistage membrane distillation for
672 water desalination. *Desalination* 437, 175–183.
673 <https://doi.org/10.1016/J.DESAL.2018.03.012>

674 Khayet, M., 2011. Membranes and theoretical modeling of membrane distillation: A review.
675 *Adv. Colloid Interface Sci.* 164, 56–88. <https://doi.org/10.1016/j.cis.2010.09.005>

676 Khayet, M., Velázquez, A., Mengual, J.I., 2004. Direct contact membrane distillation of humic
677 acid solutions. *J. Memb. Sci.* 240, 123–128. <https://doi.org/10.1016/j.memsci.2004.04.018>

678 Kim, J., Hong, S., 2018. A novel single-pass reverse osmosis configuration for high-purity
679 water production and low energy consumption in seawater desalination. *Desalination* 429,
680 142–154. <https://doi.org/10.1016/j.desal.2017.12.026>

681 Kolokassidou, C., Pashalidis, I., Costa, C.N., Efstathiou, A.M., Buckau, G., 2007. Thermal
682 stability of solid and aqueous solutions of humic acid. *Thermochim. Acta* 454, 78–83.
683 <https://doi.org/10.1016/j.tca.2006.12.022>

684 Lipczynska-Kochany, E., 2018. Humic substances, their microbial interactions and effects on
685 biological transformations of organic pollutants in water and soil: A review. *Chemosphere*

686 202, 420–437. <https://doi.org/10.1016/J.CHEMOSPHERE.2018.03.104>

687 Liu, S., Lim, M., Fabris, R., Chow, C., Chiang, K., Drikas, M., Amal, R., 2008. Removal of
688 humic acid using TiO₂ photocatalytic process – Fractionation and molecular weight
689 characterisation studies. *Chemosphere* 72, 263–271.
690 <https://doi.org/10.1016/J.CHEMOSPHERE.2008.01.061>

691 Meng, S., Ye, Y., Mansouri, J., Chen, V., 2014. Fouling and crystallisation behaviour of
692 superhydrophobic nano-composite PVDF membranes in direct contact membrane
693 distillation. *J. Memb. Sci.* 463, 102–112. <https://doi.org/10.1016/j.memsci.2014.03.027>

694 Miller, J.N., Miller, J.C., Maté Jiménez, C., Izquierdo Hornillos, R., 2002. *Estadística y*
695 *quimiometría para química analítica*. Prentice Hall.

696 Mostafa, M.G., Zhu, B., Cran, M., Dow, N., Milne, N., Desai, D., Duke, M., 2017. Membrane
697 distillation of meat industry effluent with hydrophilic polyurethane coated
698 polytetrafluoroethylene membranes. *Membranes (Basel)*. 7, 55.
699 <https://doi.org/10.3390/membranes7040055>

700 Myat, D.T., Mergen, M., Zhao, O., Stewart, M.B., Orbell, J.D., Gray, S., 2012. Characterisation
701 of organic matter in IX and PACl treated wastewater in relation to the fouling of a
702 hydrophobic polypropylene membrane. *Water Res.* 46, 5151–5164.
703 <https://doi.org/10.1016/j.watres.2012.06.054>

704 Naidu, G., Jeong, S., Kim, S.J., Kim, I.S., Vigneswaran, S., 2014. Organic fouling behavior in
705 direct contact membrane distillation. *Desalination* 347, 230–239.
706 <https://doi.org/10.1016/j.desal.2014.05.045>

707 Naidu, G., Jeong, S., Vigneswaran, S., 2015. Interaction of humic substances on fouling in
708 membrane distillation for seawater desalination. *Chem. Eng. J.* 262, 946–957.
709 <https://doi.org/10.1016/J.CEJ.2014.10.060>

710 Pal, P., Manna, A.K., 2010. Removal of arsenic from contaminated groundwater by solar-driven

711 membrane distillation using three different commercial membranes. *Water Res.* 44, 5750–
712 5760. <https://doi.org/10.1016/j.watres.2010.05.031>

713 Prisciandaro, M., Capocelli, M., Piemonte, V., Barba, D., 2016. Process analysis applied to
714 water reuse for a “closed water cycle” approach. *Chem. Eng. J.* 304, 602–608.
715 <https://doi.org/10.1016/J.CEJ.2016.06.134>

716 Qin, W., Xie, Z., Ng, D., Ye, Y., Ji, X., Gray, S., Zhang, J., 2018. Comparison of colloidal silica
717 involved fouling behavior in three membrane distillation configurations using PTFE
718 membrane. *Water Res.* 130, 343–352. <https://doi.org/10.1016/J.WATRES.2017.12.002>

719 Qtaishat, M., Khayet, M., Matsuura, T., 2009. Novel porous composite hydrophobic/hydrophilic
720 polysulfone membranes for desalination by direct contact membrane distillation. *J. Memb.*
721 *Sci.* 341, 139–148. <https://doi.org/10.1016/J.MEMSCI.2009.05.053>

722 Roccaro, P., Vagliasindi, F.G.A., Korshin, G. V., 2009. Changes in NOM Fluorescence Caused
723 by Chlorination and their Associations with Disinfection by-Products Formation. *Environ.*
724 *Sci. Technol.* 43, 724–729. <https://doi.org/10.1021/es801939f>

725 Rodríguez, F.J., Schlenger, P., García-Valverde, M., 2014. A comprehensive structural
726 evaluation of humic substances using several fluorescence techniques before and after
727 ozonation. Part I: Structural characterization of humic substances. *Sci. Total Environ.* 476–
728 477, 718–730. <https://doi.org/10.1016/J.SCITOTENV.2013.11.150>

729 Silva, T.L.S., Morales-Torres, S., Esteves, C.M.P., Ribeiro, A.R., Nunes, O.C., Figueiredo, J.L.,
730 Silva, A.M.T., 2018. Desalination and removal of organic micropollutants and
731 microorganisms by membrane distillation. *Desalination* 437, 121–132.
732 <https://doi.org/10.1016/J.DESAL.2018.02.027>

733 Villalobos García, J., Dow, N., Milne, N., Zhang, J., Naidoo, L., Gray, S., Duke, M., 2018.
734 Membrane Distillation Trial on Textile Wastewater Containing Surfactants Using
735 Hydrophobic and Hydrophilic-Coated Polytetrafluoroethylene (PTFE) Membranes.

736 Membranes (Basel). 8, 31. <https://doi.org/10.3390/membranes8020031>

737 Voulvoulis, N., 2018. Water reuse from a circular economy perspective and potential risks from
738 an unregulated approach. *Curr. Opin. Environ. Sci. Heal.* 2, 32–45.
739 <https://doi.org/10.1016/j.coesh.2018.01.005>

740 Wagner, M., Schmidt, W., Imhof, L., Grübel, A., Jähn, C., Georgi, D., Petzoldt, H., 2016.
741 Characterization and quantification of humic substances 2D-Fluorescence by usage of
742 extended size exclusion chromatography. *Water Res.* 93, 98–109.
743 <https://doi.org/10.1016/J.WATRES.2016.01.050>

744 Wang, K., Hou, D., Wang, J., Wang, Z., Tian, B., Liang, P., 2018. Hydrophilic surface coating
745 on hydrophobic PTFE membrane for robust anti-oil-fouling membrane distillation. *Appl.*
746 *Surf. Sci.* 450, 57–65. <https://doi.org/10.1016/J.APSUSC.2018.04.180>

747 Wang, Z., Wu, Z., Tang, S., 2009. Characterization of dissolved organic matter in a submerged
748 membrane bioreactor by using three-dimensional excitation and emission matrix
749 fluorescence spectroscopy. *Water Res.* 43, 1533–1540.
750 <https://doi.org/10.1016/j.watres.2008.12.033>

751 Warsinger, D.M., Swaminathan, J., Morales, L.L., Lienhard V, J.H., 2018. Comprehensive
752 condensation flow regimes in air gap membrane distillation: Visualization and energy
753 efficiency. *J. Memb. Sci.* 555, 517–528. <https://doi.org/10.1016/j.memsci.2018.03.053>

754 Wijekoon, K.C., Hai, F.I., Kang, J., Price, W.E., Cath, T.Y., Nghiem, L.D., 2014. Rejection and
755 fate of trace organic compounds (TrOCs) during membrane distillation. *J. Memb. Sci.* 453,
756 636–642.

757 Woo, Y.C., Tijing, L.D., Shim, W.-G., Choi, J.-S., Kim, S.-H., He, T., Drioli, E., Shon, H.K.,
758 2016. Water desalination using graphene-enhanced electrospun nanofiber membrane via
759 air gap membrane distillation. *J. Memb. Sci.* 520, 99–110.
760 <https://doi.org/10.1016/J.MEMSCI.2016.07.049>

761 Xu, J., Singh, Y.B., Amy, G.L., Ghaffour, N., 2016. Effect of operating parameters and
762 membrane characteristics on air gap membrane distillation performance for the treatment
763 of highly saline water. *J. Memb. Sci.* 512, 73–82.
764 <https://doi.org/10.1016/j.memsci.2016.04.010>

765 Zheng, R., Chen, Y., Wang, J., Song, J., Li, X.-M., He, T., 2018. Preparation of omniphobic
766 PVDF membrane with hierarchical structure for treating saline oily wastewater using
767 direct contact membrane distillation. *J. Memb. Sci.* 555, 197–205.
768 <https://doi.org/10.1016/J.MEMSCI.2018.03.041>

769 Ziolkowska, J.R., Reyes, R., 2016. Impact of socio-economic growth on desalination in the US.
770 *J. Environ. Manage.* 167, 15–22. <https://doi.org/10.1016/J.JENVMAN.2015.11.013>

771

28 **Keywords:** humic acid, air gap membrane distillation, water gap membrane distillation, organic
29 matter, diffusion, seawater.

30 **1. Introduction**

31 Water shortages and the loss in water quality are one of the main common global problems
32 humanity faces (Anand et al., 2018; Voulvoulis, 2018). In addition, many anthropogenic
33 compounds that cannot be treated with conventional wastewater treatments can be found in
34 natural waters, posing a significant risk to the environment and to human health (Biel-Maeso et
35 al., 2018; Han et al., 2017; Herce-Sesa et al., 2018; Wagner et al., 2016).

36 Of particular interest in water quality are natural organic matter (NOM) compounds which is
37 present in natural water systems. NOM compounds are derived from the degradation of plants,
38 animals, and microorganisms by chemical, biological and photochemical reactions. Among the
39 compounds making up NOM, humic substances (HS) are important since they are the major
40 carbon pool in the biosphere. Of the NOM presents in natural waters, up to 50% consist of HS
41 and they are the main organic compounds in seawater (Lipczynska-Kochany, 2018; Naidu et al.,
42 2015; Rodríguez et al., 2014).

43 HS are complex and heterogeneous mixtures of a wide range of molecular weight species. The
44 two main categories of HS are fulvic acids (FA) and humic acids (HA), and can be
45 distinguished in function of their solubility at pH 1 where the latter often form colloids because
46 of their large size (Rodríguez et al., 2014; Wagner et al., 2016). Although HS do not cause any
47 known adverse effects for human health, they are undesirable substances in water treatment and
48 they can play a fundamental role as indicators of water quality. HS contributes to odor, color,
49 taste and acidity problems in water supplies. Furthermore, HS, and especially HA, lead to a
50 greater spending on disinfection when chlorination is used as they are precursors of toxic
51 disinfection byproducts (DBPs) such as trihalomethanes (THMs) and haloacetic acids (HAAs)
52 (Liu et al., 2008; Roccaro et al., 2009). Finally, HS have been identified as one of the major
53 compounds responsible for fouling in membrane processes as well as the complexes formation

54 with a multitude of metal ions and organic pollutants promoting the formation of biofilm in
55 water pipes (Bond et al., 2012; Chowdhury et al., 2016; Jermann et al., 2007; Liu et al., 2008;
56 Roccaro et al., 2009). Therefore, HA and its behavior through a new proposed water treatment
57 technology is important to be investigated.

58 Water desalination and reuse technologies have great potential to address the problems
59 associated with water shortages and water quality by use of non-conventional water sources.
60 These desalination technologies are mainly based on membrane and/or thermal processes, or a
61 combination of both in a process train while reuse technologies are mainly based on membrane
62 processes. Some of these technologies are reverse osmosis (RO), electrodialysis, nanofiltration
63 (NF), multiple-effect distillation (MED) and multi-stage flash distillation (MSF). An alternative
64 process combining membranes with thermal desalination is membrane distillation (MD)
65 (Criscuoli and Carnevale, 2015; Ghaffour et al., 2013; Kim and Hong, 2018; Prisciandaro et al.,
66 2016; Ziolkowska and Reyes, 2016). MD is a thermally driven separation using a membrane as
67 a barrier for saline liquid water, while being permeable to fresh water vapor. In this way, the
68 vapor pressure between both sides of this membrane, being microporous and hydrophobic in
69 order to fulfill the liquid barrier and vapor permeable requirement, is the driving force in this
70 separation process.

71 The advantages of MD proposed include the use of small and compact equipment and very low
72 working pressures which could lead to lower material costs and greater process safety compared
73 to other conventional technologies (Alkhudhiri et al., 2012a; Essalhi and Khayet, 2015; Khalifa,
74 2015). Additionally, MD can use low-grade and waste heat as well as alternative energy
75 sources, increasing energy efficiency. In terms of membrane performance, the fouling of the
76 membranes can be lower than in other membrane processes while a very high water quality is
77 produced because of the 100% theoretical rejection of non-volatile components (Alkhudhiri and
78 Hilal, 2017; Guillen-Burrieza et al., 2014). Among MD configurations, commonly investigated
79 modes include direct contact MD (DCMD), air gap MD (AGMD) and water gap MD (WGMD).
80 In DCMD, feed and cooling water are in contact with the membrane surfaces. In this way, the

81 transmembrane flow (membrane flux) is high but there are also high heat losses by conduction.
82 As a result of this setup, obtaining an isolated distillate is not possible, since it is mixed with the
83 cooling water. This is avoided with the AGMD setup as the distillate can be obtained separately
84 from the cooling water, however the drawback is membrane flux is lower than in DCMD.
85 Another configuration, WGMD, emerged as an improvement over these limitations of DCMD
86 and AGMD. In WGMD, the gap is filled with distilled water. This configuration offers an
87 improvement in the permeate flow in comparison with AGMD and it allows a separate distillate
88 to be obtained, unlike DCMD (Francis et al., 2013; González et al., 2017).

89 These MD advantages make it a promising alternative to conventional desalination and water
90 reuse technologies for many environmental and industrial applications (Amaya-Vías et al.,
91 2018; Cui et al., 2018; Silva et al., 2018). Nevertheless, MD is not fully commercialized and
92 implemented by industry (Khayet, 2011; Qtaishat et al., 2009), since many aspects have still not
93 been studied in detail; for example, the effect of organic matter (OM) and HA in the MD
94 process. Many authors have focused their studies on the MD fouling and the HA influence in
95 the rejection of different substances. However, the permeation of HA through the membrane
96 into the permeate has so far only been observed as a side result in these DCMD fouling studies
97 (Han et al., 2017; Khayet et al., 2004; Meng et al., 2014; Naidu et al., 2015, 2014; Wijekoon et
98 al., 2014).

99 In view of their importance and consequences of HA presence in treated water supplies, the
100 reason for the diffusion of this non-volatile molecule of large size into the treated MD permeate
101 is clearly of interest to scientists and engineers. This work is therefore dedicated to explore the
102 behavior of HA through the membrane in AGMD and WGMD configurations with the view to
103 understand its diffusion mechanisms. Studies have been carried out in order to analyze the pure
104 permeate and evaluate the behavior of the HA for different membranes, operating temperatures
105 and flow rates. Different conditions have been studied with synthetic water as well as real
106 seawater from a local seawater source.

107 **2. Materials and methods**

108 *2.1. Reagents and membranes*

109 Synthetic water composition used in this study was set at 1 g L⁻¹ sodium chloride (NaCl)
110 EMSURE® (Merck, Germany), 8 mM (~0.88 g L⁻¹) calcium chloride ≥96% anhydrous (CaCl₂,
111 Sigma-Aldrich), 100 mg L⁻¹ humic acid sodium salt (H16752 Sigma-Aldrich) and deionized
112 water, in order to simulate surface water with a typical OM model, according to Han et al (Han
113 et al., 2017). In addition, real seawater was obtained from Port Phillip (Melbourne, Australia) to
114 study NOM behavior in MD.

115 A hydrophobic, microporous membrane from Ningbo Changqi Porous Membrane Technology
116 Co, Ltd. (Ningbo, China) was used in the MD tests. The membrane consisted of a thin
117 polytetrafluoroethylene (PTFE) active layer (40 μm) on top of a polypropylene (PP) support
118 layer, with a nominal pore size and total thickness of 0.5 μm and 106 μm, respectively.
119 Although this PTFE membrane was used as a reference throughout the study, another three
120 membranes were used in order to study the HA behavior with different materials and membrane
121 characteristics.

122 In this way, a hydrophobic polyethylene (PE) membrane and omniphobic PE membrane without
123 support layer from Aquastill were used, featuring both a nominal pore size of 0.2 μm and
124 thickness of 63 μm and 67 μm, respectively. In addition, a hydrophilic polyurethane (PU)
125 coated hydrophobic PTFE membrane from Australian Textile Mills (ATM) was used. PU layer
126 has a pore size less than 2 nm and the PTFE layer, 0.35 μm with a total membrane thickness of
127 164 μm. Some additional membrane characteristics used in this study are reported elsewhere
128 (Mostafa et al., 2017; Qin et al., 2018; Villalobos García et al., 2018).

129 *2.2. Experimental MD setup*

130 MD testing was conducted in a laboratory system in AGMD and WGMD modes using a similar
131 setup reported elsewhere (Amaya-Vías et al., 2018; Francis et al., 2013; Khalifa, 2015). Briefly,
132 MD system consisted of a co-current flat sheet acrylic membrane module with an effective
133 membrane area of 0.018 m², a feed tank, a cooling tank and two peristaltic pumps (Masterflex®

134 L/S 77800-62, Cole-Parmer). One spacer (thickness = 0.8 mm, porosity = 0.87) was placed on
135 feed side to enhance the turbulence of the feed stream. In addition, for both MD configurations a
136 3 mm gap made with a perforated plate was used to support the membrane and prevent the
137 membrane from possible deformation or damage (Alkudhiri et al., 2012b; Attia et al., 2017b,
138 2017a; Duong et al., 2016; Khalifa, 2015; Khalifa and Alawad, 2018; Pal and Manna, 2010; Xu
139 et al., 2016). Both tanks were covered to minimize losses by evaporation and a mass balance
140 was calculated for all experiments. A heater (Thermo Scientific Neslab RTE7) and a chiller
141 (PolyScience®) maintained the temperatures configured in the feed and cooling tanks,
142 respectively. The permeate was collected in a measuring cylinder and the permeate flow was
143 measured by the volumetric method, as described by Dow et al. (Dow et al., 2016). A simplified
144 schematic flowsheet is shown in Fig.1.

145 Electrical conductivity (EC) and pH of the water samples were determined using a portable
146 multi meter (Hach HQ40D, Loveland, CO, USA).

147 Several parameters were calculated based on experimental measurements. The first is the
148 permeate flow rate ($L h^{-1}$) used to determine total flux, J ($L h^{-1} m^{-2}$) by Eq. (1):

$$J = \frac{V_{perm}}{A \cdot \Delta t} \quad (1)$$

149 Where V_{perm} is the permeate volume produced in the time interval (L), A is the membrane area
150 (m^2) and Δt is the time interval (h).

151 HA flux, J_{HA} ($mg_{HA} h^{-1} m^{-2}$), with respect to total flux in both MD configurations was also
152 calculated as in Eq. (2), where $[HA]$ is the HA concentration ($mg_{HA} L^{-1}$) in permeate collected
153 over time interval Δt , using the TOC calibration equation to specify the $[HA]$. Limits of
154 detection (LOD) were calculated as $3\sigma_b/m$ where σ_b is the standard deviation of ten blank
155 samples and m the slope of the calibration curve. Additionally, limit of quantification (LOQ)
156 was calculated as $10\sigma_b/m$ (Miller et al., 2002).

157

$$J_{HA} = [HA] \cdot J \quad (2)$$

158 Finally, rejection factor (RF) for a variable was calculated by Eq. (3):

159

$$RF (\%) = \left(\frac{C_{feed} - C_{perm}}{C_{feed}} \right) \cdot 100 \quad (3)$$

160 Where C_{feed} and C_{perm} are values in the feed and permeate, respectively. This equation was used
161 to calculate the EC rejection factor (RF_{EC}) and Non Purgeable Organic Carbon (NPOC)
162 rejection factor (RF_{NPOC}) using experimentally obtained EC and NPOC values respectively.

163 For the experimental design, real seawater was tested with the purpose of checking the presence
164 of NOM in MD permeate. It was decided to use seawater for two main reasons. Firstly, seawater
165 desalination is one of the main applications in which MD can be potentially used. Secondly,
166 taking into account that HS are the main component of the NOM in seawater (Naidu et al.,
167 2015; Rodríguez et al., 2014), HA flux can be evaluated easily, assuming that all NOM in
168 seawater samples was HA. Therefore, HA flux is estimated by the TOC-HA calibration curves
169 used for synthetic water. Then to ensure tests with a consistent feed, the seawater was replaced
170 with a synthetic saline water in order to study the influence of the both sides (feed and cooling)
171 temperatures, operation flow rates and the different membranes described previously. The initial
172 feed volume was 2.5 L and the operation time for each test was 4 h being sufficient time to
173 show steady state performance. Permeate samples were taken every hour, while feed side was
174 monitored taking a sample at the start and at the end of the test. New membranes were used for
175 each operating condition.

176 Firstly, AGMD and WGMD tests were performed at different temperatures, flow rates and cross
177 flow velocity (CFV) using four different MD membranes as indicated in Table 1.

178 **Table 1.** Operating conditions (temperatures, flow rates, CFV and MD membranes) studied in
 179 AGMD and WGMD tests.

Temperature tests at 90 L h⁻¹ (0.034 m s⁻¹) cross flow using PTFE membrane

Feed temperature (°C) / Cooling temperature (°C)

50 / 18 60 / 18 70 / 18 70 / 35

Flow rate tests at 70°C (feed) and 18°C (permeate) using PTFE membrane

Flow rate (L h⁻¹) / CFV (m s⁻¹)

60 / 0.023 75 / 0.029 90 / 0.034 105 / 0.04 120 / 0.046

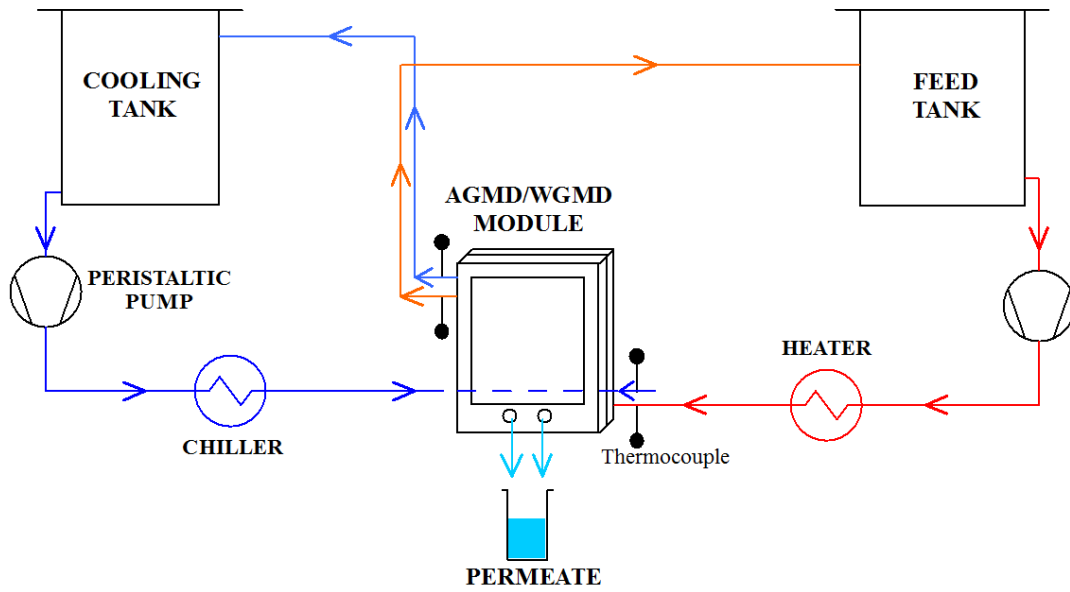
Membrane tests at 70°C (feed), 18°C (permeate) and 90 L h⁻¹ (0.034 m s⁻¹) cross flow

PTFE	PTFE-PU	PE-hydrophobic	PE-omniphobic
------	---------	----------------	---------------

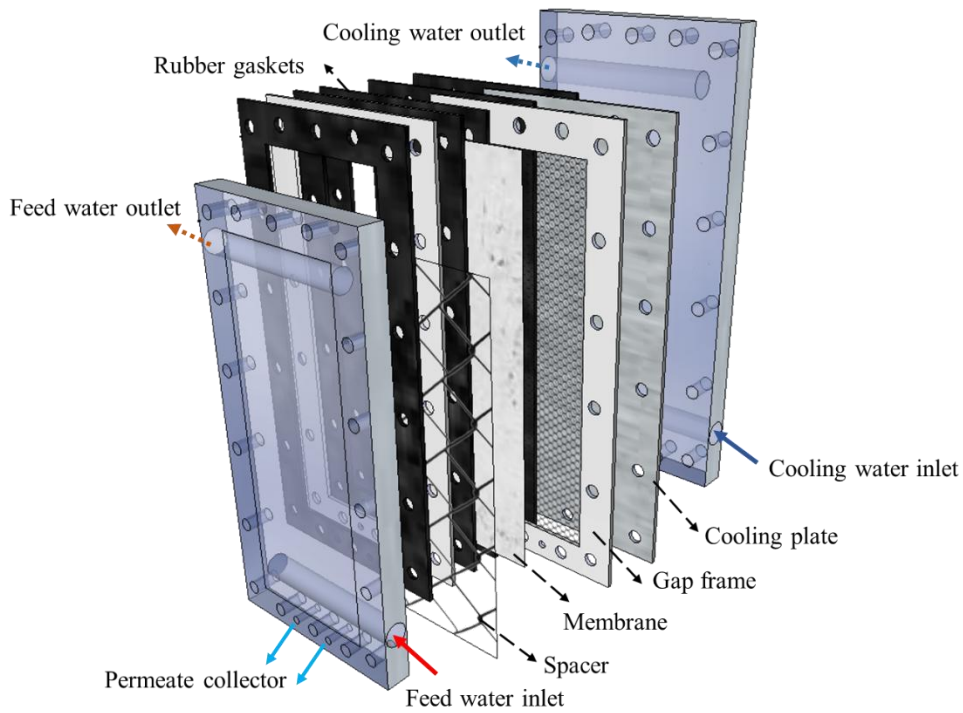
180

181 Further experiments were conducted to better understand the behavior of HA in AGMD, by
 182 implementing a double gap width (total thickness of 6 mm) into the module. In this case, feed
 183 water was slightly changed using deionized water and 50 mg L⁻¹ of HA to avoid saline
 184 interferences and a high HA concentration. This mode was compared to AGMD and WGMD
 185 keeping the same feed water and the experimental conditions.

186 Finally, Naidu et al (Naidu et al., 2015) reported thermal degradation of HA where lower
 187 molecular sized HS and other organics were observed. Hence, tests using a rotary evaporator
 188 (Tokyo Rikakikai SB-650 N-N, Japan) were carried out, recreating MD tests with seawater and
 189 synthetic water in order to determine if HA presence in the permeate was because of the MD
 190 process or to a greater volatility of HA thermal degradation byproducts.



191



192

193 **Fig. 1.** Schematic co-current AGMD/WGMD setup used in this work and MD module details.

194

195 *2.3. Analytical techniques*

196 The concentration of HA in the feed and permeate was measured mainly by total organic carbon

197 analyser (TOC-V CSH, Shimadzu, Kyoto, Japan), as suggest Meng et al (Meng et al., 2014).

198 NPOC method was used for all organic carbon measurements. Complementary measurements

199 using a UV spectrophotometer (UV-1800, Shimadzu, Kyoto, Japan) at the wavelength of 254
200 nm were used, according to Han and Myat et al (Han et al., 2017; Myat et al., 2012). Both
201 instruments were calibrated, resulting in a linear relationship in the HA concentration range of
202 0-100 mg L⁻¹, with a regression coefficient of 0.999 and 0.998, respectively. Furthermore,
203 fluorescence excitation-emission spectra (EEM) were recorded on a fluorescence
204 spectrophotometer (Horiba Scientific Aqualog, Kyoto, Japan). These spectra were compared
205 with previous studies related to HA and OM (Rodríguez et al., 2014; Wang et al., 2009).

206 Contact angle with deionized water and with HA solution was examined for each membrane,
207 using a Contact Angle Analyser (Kruss DSA25). An average of four measurements at different
208 locations of the membrane were taken by the static sessile drop method and the average value is
209 reported.

210 Finally, the various MD tests and sample measurements were carried out at least in triplicate, in
211 order to demonstrate the confidence of the results obtained. In addition, all results were verified
212 with calibration curves, as well as TOC and HA flow data were found above with LOD (0.30
213 mg L⁻¹) and LOQ (0.44 mg L⁻¹) in all cases.

214 **3. Results and discussion**

215 *3.1. MD performance with real seawater and synthetic saline water with HA*

216 Results for all experiments performed with both MD configurations and feed solutions are
217 shown in Table 2. In all cases, the saline rejection factor, RF_{EC} , (based on EC measurement) was
218 above 99%. This shows that membrane wetting has likely not taken place and membranes were
219 intact during the experiments. Meanwhile RF_{NPOC} showed lower values, reaching a minimum
220 value of 33 ± 11 % and no higher than 93% in all cases. Seawater tended to show lower RF_{NPOC}
221 values suggesting a different property of the organics. The carbon and representative HA flux
222 are shown in Table 3. However the lower rejection of organics compared to EC shows that even
223 for synthetic saline water, organic material is diffusing through the membrane. In the case of

224 synthetic water where the only organic material added was HA, it confirms that this diffusion is
 225 by HA molecules.

226 **Table 2.** Average permeate EC, NPOC, RF_{EC} and RF_{NPOC} for different MD configuration and
 227 feed water. Initial conditions for feed seawater: EC: $44057 \pm 1858 \mu\text{S cm}^{-1}$, NPOC: 2.6 ± 0.2
 228 mg L^{-1} . Initial conditions for feed synthetic water: EC: $3340 \pm 180 \mu\text{S cm}^{-1}$, NPOC: 16.3 ± 1.8
 229 mg L^{-1} . TOC LOD: 0.30 mg L^{-1} ; TOC LOQ: 0.44 mg L^{-1} .

		EC	NPOC	RF_{EC}	RF_{NPOC}
		$\mu\text{S cm}^{-1}$	mg L^{-1}	%	%
AGMD	Seawater	40 ± 21	1.7 ± 0.3	99.9 ± 0.1	33 ± 11
	Synthetic water	14 ± 1	1.7 ± 0.7	99.6 ± 0.0	90 ± 4
WGMD	Seawater	51 ± 20	0.8 ± 0.2	99.9 ± 0.0	68 ± 7
	Synthetic water	3 ± 0	1.2 ± 0.3	99.9 ± 0.0	93 ± 2

230

231 **Table 3.** Carbon and representative HA flux for MD test using real seawater and average
 232 results (all operating conditions) for MD test using synthetic saline water with HA. Feed and
 233 cooling temperatures for seawater: 70°C and 18°C , respectively. Steady state fluxes for
 234 seawater tests: $3.3 \pm 0.2 \text{ L h}^{-1} \text{ m}^{-2}$ for AGMD and $8.1 \pm 1.0 \text{ L h}^{-1} \text{ m}^{-2}$ for WGMD.

235

Mode	Seawater		Synthetic water	
	Carbon Flux $\text{mgC h}^{-1} \text{ m}^{-2}$	HA Flux $\text{mgHA h}^{-1} \text{ m}^{-2}$	Carbon Flux $\text{mgC h}^{-1} \text{ m}^{-2}$	HA Flux $\text{mgHA h}^{-1} \text{ m}^{-2}$
AGMD	5.9 ± 1.4	21.5 ± 5.4	6.0 ± 2.5	21.6 ± 9.7
WGMD	6.4 ± 1.0	19.7 ± 4.4	8.2 ± 2.7	27.9 ± 10.3

236

237 3.2. Rotary evaporator tests with real seawater and synthetic saline water with HA

238 Results obtained in the rotary evaporator tests are shown in Table 4. The experiments were
 239 carried out under the same conditions as in MD for convenient comparison. EC was measured
 240 in some permeate samples, where EC values below $3 \mu\text{S cm}^{-1}$ were obtained in all cases. The
 241 RF_{EC} therefore reached where $>99\%$ and compared well with the MD tests shown in Table 2.
 242 However a major difference was to NPOC rejection, where the distillate concentrations were
 243 very similar to the blank (deionized water) in all cases showing that HA compounds and OM
 244 contained in both synthetic water and seawater are not volatile. In addition, it is verified that HS

245 thermal degradation byproducts do not pass into the vapor phase. In this sense, HA diffusion
 246 process through the membrane is inherent to the MD process. Therefore the next part of this
 247 work will be to explore the effect of typical MD operating conditions on the diffusion of HA.

248 **Table 4.** NPOC values for seawater and synthetic water using rotary evaporator.

	Seawater			Synthetic water		
	Feed	Condensate	Blank	Feed	Condensate	Blank
NPOC mg L ⁻¹	2.6 ± 0.2	0.4 ± 0.2	0.4 ± 0.2	16.3 ± 1.8	0.6 ± 0.1	0.4 ± 0.1

249

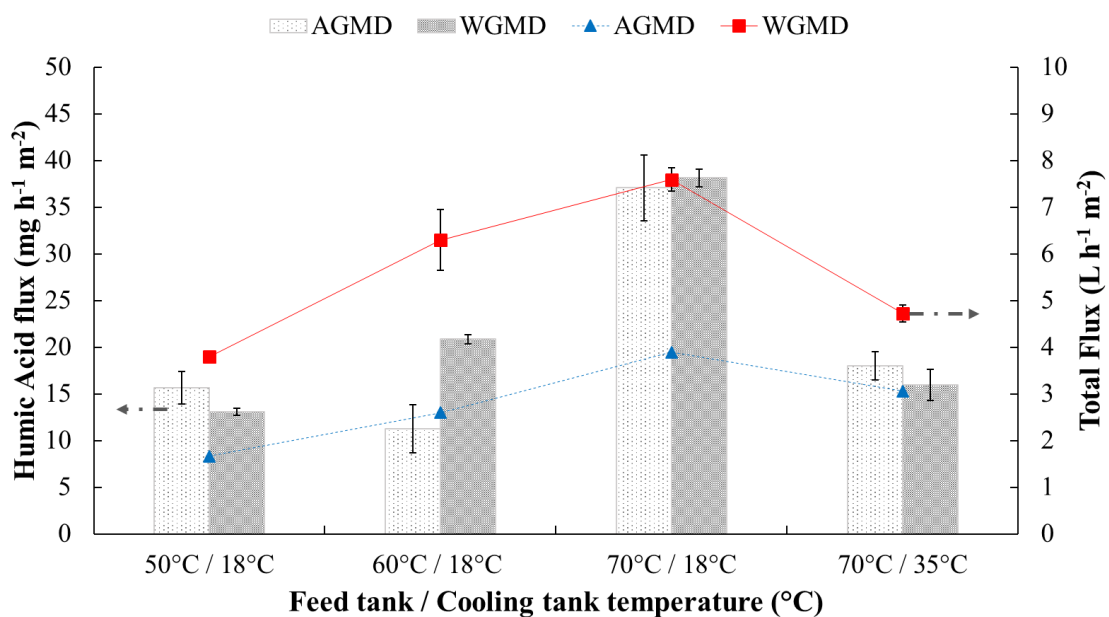
250 *3.3. Effect of MD operating conditions on HA diffusion*

251 *3.3.1. Effect of operating temperatures*

252 Fig.2 shows the influence of different operating temperatures on the HA flux through the
 253 membrane. As it can be seen, HA flux was increased (from 15.6 to 37.1 mg h⁻¹ m⁻² for AGMD
 254 and 13.1 to 38.1 mg h⁻¹ m⁻² for WGMD) with higher feed temperatures in the same manner as
 255 the total flux (from 1.7 to 3.9 L h⁻¹ m⁻² for AGMD and 3.8 to 7.6 L h⁻¹ m⁻² for WGMD).
 256 Nevertheless, when the cooling temperature set to 35°C keeping feed temperature at 70°C, total
 257 flux decreased (3.1 L h⁻¹ m⁻² and 4.7 L h⁻¹ m⁻² for AGMD and WGMD, respectively) since there
 258 was a lower vapor pressure across the membrane. Likewise, HA flux decreased to 18.0 mg h⁻¹
 259 m⁻² for AGMD and 16.0 mg h⁻¹ m⁻² for WGMD. Based on this result, it appears that HA flux
 260 generally follows total flux, supporting the concept that HA is entrained through the membrane
 261 with water following the model proposed by Meng et al (Meng et al., 2014). However it is not a
 262 direct correlation since there was little or no increase in HA flux from 50°C to 60°C, but a large
 263 increase occurred from 60°C to 70°C. Meanwhile water flux increase was proportionately
 264 similar at each temperature step (cases of 18°C permeate cycle temperatures). This is evidence
 265 that water and HA diffusion are not entirely connected which will be further explored later in
 266 this paper. Comparing the HA flux obtained for AGMD and WGMD, both MD configurations
 267 showed a similar behavior where it should be expected no non-volatile HA would be present at
 268 all in AGMD permeate. In this way, several types of condensation may occur in AGMD

269 systems as is suggested by Warsinger et al (Warsinger et al., 2018) and therefore, the presence
 270 of HA flux in AGMD suggests liquid contact between the membrane and condensing plate.
 271 Additionally, in Figure 2 a discrepancy of HA fluxes for AGMD and WGMD in the test at a
 272 temperature of 60°C is reported. This performance could be also attributed to liquid contact
 273 between membrane and condensing plate (water bridging) in AGMD. Thus, water bridging
 274 could be different as the flux is lower, but when more water flux occurs, the risk of bridging
 275 increases rapidly, potentially due to rapid coalescence of condensed water clusters. This is
 276 potentially a reason why it rose suddenly for AGMD when water flux is higher.

277 Looking more closely at the chemistry, pH is known to play an important role in the behavior
 278 and solubility of HA (Khayet et al., 2004). However no large differences in pH were observed
 279 in the experiments carried out using synthetic water. The pH on average for AGMD was $6.39 \pm$
 280 0.26 while for WGMD was 6.66 ± 0.21 . Feed pH was 6.81 ± 0.31 . According to the results
 281 obtained, it can be assumed that HA behavior is not attributed to pH changes between feed and
 282 permeate. In terms of EC rejection, AGMD was slightly less effective than WGMD but both
 283 were >99%. The salinity may also play a role in the HA diffusion, where future work could
 284 consider the effect of total dissolved solids concentration, including effects of other trace
 285 minerals including calcium and iron.



286

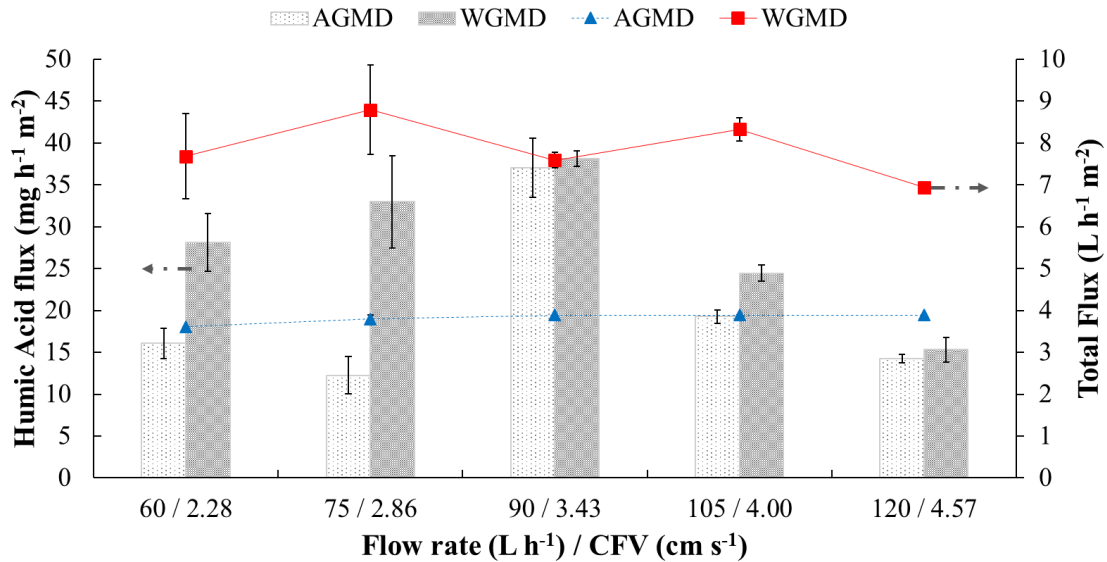
287 **Fig. 2.** HA flux obtained for PTFE membrane and both MD configurations at different operating
288 temperatures. Total flux is represented by lines graphed on the secondary axis. Feed and cooling
289 cycle flow rate: 90 L h⁻¹. Feed water: 1 g L⁻¹ NaCl, 0.88 g L⁻¹ CaCl₂ and 100 mg L⁻¹ HA. PTFE
290 membrane with effective area of 0.018 m². Due to low errors on some points, error bars cannot
291 be seen.

292

293 3.3.2. *Effect of cross flow rate*

294 Figure 3 shows the total flux and HA flux from MD testing on synthetic saline water with HA at
295 varied cross flows with fixed feed and permeate temperature conditions. AGMD total flux was
296 mostly constant (3.9 L m⁻² h⁻¹) for flow rates of 90, 105 and 120 L h⁻¹ but slightly increase by
297 7.75% over the entire range. WGMD showed large variations in total flux for flow rates of 60
298 and 75 L h⁻¹ but was generally higher than AGMD with flux values between (7 L m⁻² h⁻¹ and 9 L
299 m⁻² h⁻¹). These total flux and HA flux variations in WGMD could be caused by the specific
300 operational features. For example, in WGMD, permeate is collected by overflow of the water
301 gap while AGMD is collected by gravity. Therefore, as a possible effect, WGMD permeate is
302 affected by the feed flow pushing on the membrane surface and in turn, membrane movement
303 generates a pulse effect in the gap. In this sense, flow rates greater than 75 L h⁻¹ generated a
304 constant total flux in all experiments. Nevertheless, for the studied flow rates of 60 L h⁻¹ and 75
305 L h⁻¹, the membrane pulse was lower, and consequently, total flux was more variable over time.
306 In any case, errors in WGMD did not show a discernible trend, and the total flux overall trend
307 for both MD configurations indicated a low sensitivity of the total flux to CFV within the range
308 studied. However, considering this more carefully, temperature must also be considered with
309 varying cross flow as it is a key factor for MD process. In all cases, high EC rejections were
310 obtained (99.9% for WGMD and 99.6% for AGMD) and pH values (6.5 and 6.4 for WGMD
311 and AGMD, respectively) were similar and comparable to temperature tests. In the studied
312 range, a change in flow rates keeping temperatures constant does not significantly affect the
313 vapor pressure difference across the membrane and consequently, total fluxes are almost
314 constant. This does not mean that in other flow rate conditions, the reduced polarization effects
315 and a higher temperature profile uniformity, added to a thermal energy increase by higher CFV,
316 would in turn substantially increase the total flux.

317 Looking at HA fluxes the behavior was independent to that of total flux and showed a unique
 318 effect. Therefore, it has been further shown that HA can diffuse independently of water, where
 319 effects of cross flow will impact its diffusion. The functional effect cross flow has on HA
 320 diffusion may be its effect on the fluid-membrane interface (i.e. boundary layer).



321

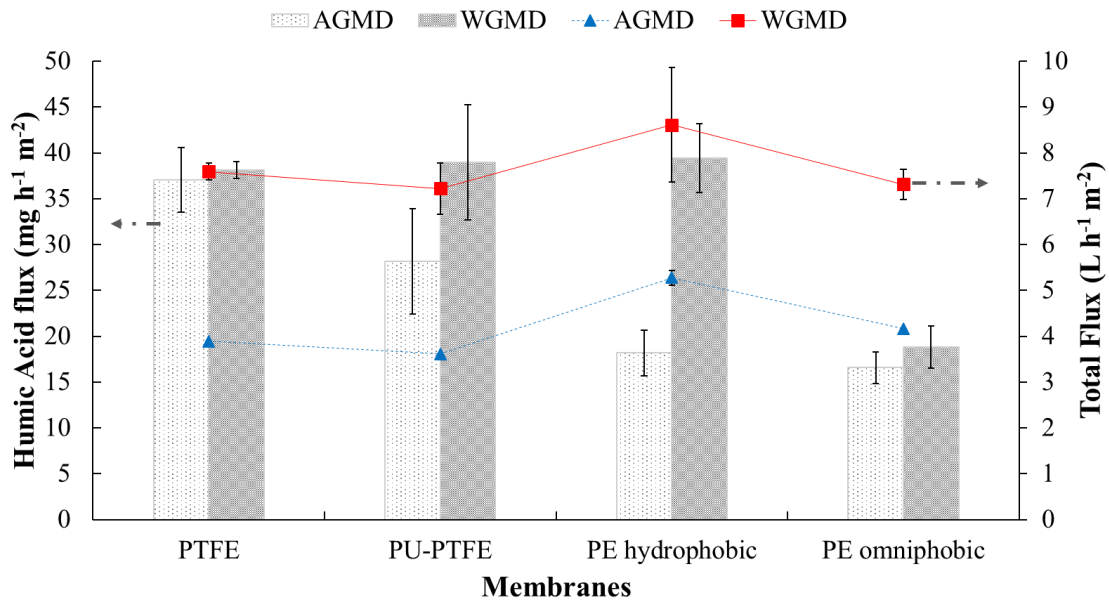
322 **Fig. 3.** HA flux obtained for PTFE membrane and both MD configurations at different flow
 323 rates and CFV. Total flux is represented by lines graph on a secondary axis. Feed and cooling
 324 temperatures: 70°C and 18°C, respectively. Feed water: 1 g L⁻¹ NaCl, 0.88 g L⁻¹ CaCl₂ and 100
 325 mg L⁻¹ HA. PTFE membrane with effective area of 0.018 m². Due to low errors on some points,
 326 error bars cannot be seen.

327

328 In these tests, HA flux showed a clear trend. At lower CFVs, 2.28 and 2.86 cm s⁻¹, HA flux for
 329 AGMD showed low values. The explanation could be related to a higher mass transfer
 330 resistance of the AGMD, as will be discussed in section 3.4. However, it peaks considerably at
 331 the middle range CFV at 3.43 cm s⁻¹. Meanwhile, HA flux for WGMD showed a similar peak at
 332 this CFV but gave higher initial values at the lower CFVs tested. For higher CFVs to 3.43 cm s⁻¹,
 333 a clearly descending trend can be observed for HA flux in both MD configurations, reaching a
 334 minimum HA flux by WGMD at CFV of 4.57 cm s⁻¹. A mechanisms of HA diffusion related to
 335 the flow across the membrane surface has become evident, which will be discussed later. The
 336 next section will consider the membrane surface chemistry to further explore the effect of the
 337 liquid-membrane surface interactions on HA flux.

338 3.3.3. Effect of membrane chemistry

339 Fig.4 shows the results for tests on the standard hydrophobic PTFE membrane compared to
 340 other membrane types to explore the influence of different materials on the HA flux in
 341 permeate. PU-PTFE (hydrophilic PU coated hydrophobic PFTE), hydrophobic PE and
 342 omniphobic PE showed similar results to the standard PTFE membranes in terms of total flux.
 343 EC rejection (99.6% AGMD and 99.9% for WGMD) and pH of AGMD and WGMD permeates
 344 (6.4 and 6.5, respectively) were similar in all cases and behavior similar to both temperature and
 345 flow rate cases. However difference were observed between the membrane chemistries for HA
 346 flux. HA flux through the PTFE membrane is highest in both AGMD and WGMD, and similar
 347 to PU-PTFE within error. Meanwhile PE hydrophobic was only similar in HA flux for WGMD
 348 mode, while AGMD mode showed HA flux was about 50% of any of these higher values. This
 349 small value was similar for PE omniphobic, uniquely in both AGMD and WGMD.



350

351 **Fig. 4.** HA flux obtained for different membranes and both MD configurations. Total flux is
 352 represented by lines graph on a secondary axis. Feed and cooling temperatures: 70°C and 18°C,
 353 respectively. Feed and cooling cycle flow rate: 90 L h⁻¹. Feed water: 1 g L⁻¹ NaCl, 0.88 g L⁻¹
 354 CaCl₂ and 100 mg L⁻¹ HA. Each membrane has an effective area of 0.018 m². Due to low errors
 355 on some points, error bars cannot be seen.

356 In relation with other membranes tested, omniphobic PE membrane with about 50% of the HA
 357 flux through PTFE in both AGMD and WGMD while at the same time as maintaining a similar

358 level of total flux. Clearly membrane chemistry is influencing the HA flux, where a
359 hydrophobic chemistry favours HA diffusion in the liquid-liquid feed-permeate contact WGMD
360 mode. This is also true for PU-PTFE where despite the hydrophilic PU coating facing the feed
361 solution, HA still diffused into the permeate through the underlying hydrophobic PTFE layer.
362 The omniphobic membrane possessed also the ability to repel hydrophobic interactions
363 indicating the HA diffusion through MD membranes is due to hydrophobic interactions between
364 the membrane and the HA molecule. The outstanding result was for the hydrophobic PE
365 membrane which gave HA fluxes for WGMD similar to the PTFE membranes, but gave lower
366 HA flux in AGMD similar to the omniphobic PE membrane. This result cannot be fully
367 explained based on the present data, and may be due to differences in the hydrophobicity of the
368 PE material compared to PTFE that yielded differences between the MD modes where AGMD
369 may have had less water bridging and in turn reduced HA flux.

370 Contact angle (CA) was measured on virgin membranes using synthetic water (1 g L⁻¹ NaCl,
371 0.88 g L⁻¹ CaCl₂ and 100 mg L⁻¹ HA) and deionized water measurement in order to confirm the
372 hydrophobicity of the membrane surfaces. A MD membrane with a water contact angle above
373 90° is considered hydrophobic (García-Fernández et al., 2015). In this way, according to water
374 CA measured, PTFE (97°) and both PE membranes (106° for hydrophobic and 122° for
375 omniphobic) exhibited hydrophobic surfaces, while hydrophilic PU-PTFE membrane showed a
376 water CA around 69° showing a hydrophilic surface, due to the PU coating on the underlying
377 hydrophobic PTFE that blocks liquid water.

378 Furthermore, CA measurements using synthetic water supported the same theory explained
379 previously using deionized water. In this way, synthetic water CA measured for each membrane
380 was 88° for PTFE, 72° for PTFE-PU, 114° for PE hydrophobic and 127° for PE omniphobic.
381 Although HA interaction with the membrane surface cannot be completely explained only by
382 the CA analysis, a trend is observed among the CA and the HA flux using synthetic water, even
383 for the PTFE-PU membrane, which is a composite membrane where only its surface facing the
384 liquid is hydrophilic.

385 In this sense, it is important to highlight the CA analysis to omniphobic PE membrane, which
386 presents the lowest values of HA flux and, in turn, the highest CA values (122° and 127° for
387 deionized water and synthetic water, respectively). These results suggest that modified
388 membranes could play an important role in OM rejection and other elements with the same
389 features. Meanwhile, the unusual result for the hydrophobic PE membrane in Figure 4 observed
390 earlier may be explained by the relatively higher CA. When the gap is filled with water in the
391 case of WGMD, HA may freely diffuse from the membrane surface into the permeate liquid. On
392 the other hand, for AGMD the more hydrophobic surface could have assisted in repelling the
393 bridging of liquid water from the permeate membrane surface across the gap to the condensing
394 plate sufficiently more than both PTFE membranes. The more intact air gap therefore acted as a
395 barrier to HA flux being more like the rotary evaporator test where HA could not be entrained
396 into the distillate through the vapour phase. Furthermore, the study of other membrane
397 properties such as thickness, porosity and tortuosity would play a role, so a detailed analysis of
398 such properties on these membranes is needed to extend our current study to explore means to
399 understand and control HA diffusion through MD membranes.

400 In conclusion, even though there are no large changes in the total flux, a clear decrease in the
401 HA flux was obtained for omniphobic PE membrane and for the high CA hydrophobic
402 membrane in AGMD mode. Therefore, according with works from other authors (Damtie et al.,
403 2018; Duong et al., 2018; Wang et al., 2018; Woo et al., 2016; Zheng et al., 2018) and the
404 results obtained in this study, we conclude that MD membranes play an important role in the
405 quality of the permeated water.

406 *3.4. HA diffusion models*

407 According to results obtained for MD tests using synthetic water, HA diffusion models can now
408 be proposed based on the key operating conditions of temperature and flow rate.

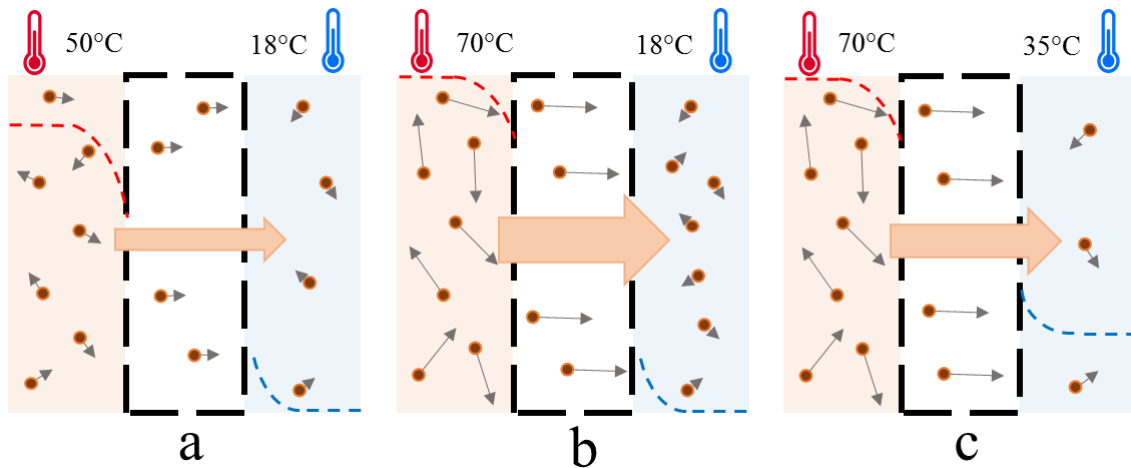
409 Experimental data suggest that the HA diffusion as a function of temperature can be explained
410 by Fick's Law. Thus, the diffusivity of HA within the membrane and the HA driving force

411 across the membrane surfaces are the main phenomena that could affect the flux. Hence, it is
412 observed that the increase in feed temperature increased the HA flux and therefore, the
413 temperature influences the HA diffusivity. However, the increase in permeate temperature
414 showed a considerable decrease in HA flux, so it seems to be strongly related to the HA driving
415 force based on the surface concentrations of HA. Taking the latter into account as well as the
416 results obtained for flux and membranes tests, it is suggested that the increase in feed
417 temperature raised the concentration of HA on the membrane surface by increasing its access
418 from the bulk to the surface, potentially from increased diffusion through the boundary layer.
419 So, when permeate temperature increased, total flux decreased and the concentration
420 polarization of HA from water flux on the feed declined. Figure 5 shows the proposed model for
421 the HA diffusion because of temperature.

422 In addition, another phenomenon could affect in a complementary way to overall HA flux, by
423 which, the adsorption of HA on the surface of the membrane decreases with the increase in
424 temperature, while the diffusivity of HA increases.

425 In this sense, the discrepancy obtained for the HA flux in AGMD at 60°C (Figure 2) could be
426 explained both to the effect of the water bridges, to the diffusion models, discussed above, and
427 to small structural changes of the HA with temperature. In the latter case, some authors
428 (Giovanela et al., 2010, 2004; Kolokassidou et al., 2007) reported that there are small changes
429 in the structure of HA resulting in a loss of mass in the temperature range of 40°C to 80°C.
430 These changes are related to the reversible and irreversible losses of different types of water
431 molecules contained in the HA. Thus, reversible structural changes occur at around 60°C, while
432 irreversible changes become important at 70°C (formation of more condensed and hydrophobic
433 polyaromatic structures) (Giovanela et al., 2010, 2004; Kolokassidou et al., 2007). Based on
434 these studies, in MD tests at temperatures of 60°C, it is suggested that HA molecules loaded
435 with water coexist with HA molecules with more condensed reversible structures. Therefore,
436 while for WGMD both types of molecules could be diffused without high resistance to
437 permeate, the heavier HA molecules would have lower diffusion because of the higher mass

438 transfer resistance of AGMD due to the air gap (Alkudhiri et al., 2012a). In addition, the effect
 439 of less water bridges in AGMD at lower fluxes (section 3.3.1) could be considerable. For these
 440 reasons, the HA flux in the AGMD is lower than the WGMD under these experimental
 441 conditions. However, there is not enough evidence to conclude if the sudden rise in HA flux at
 442 70°C is due to altered HA chemistry or an accelerated water bridging effect.

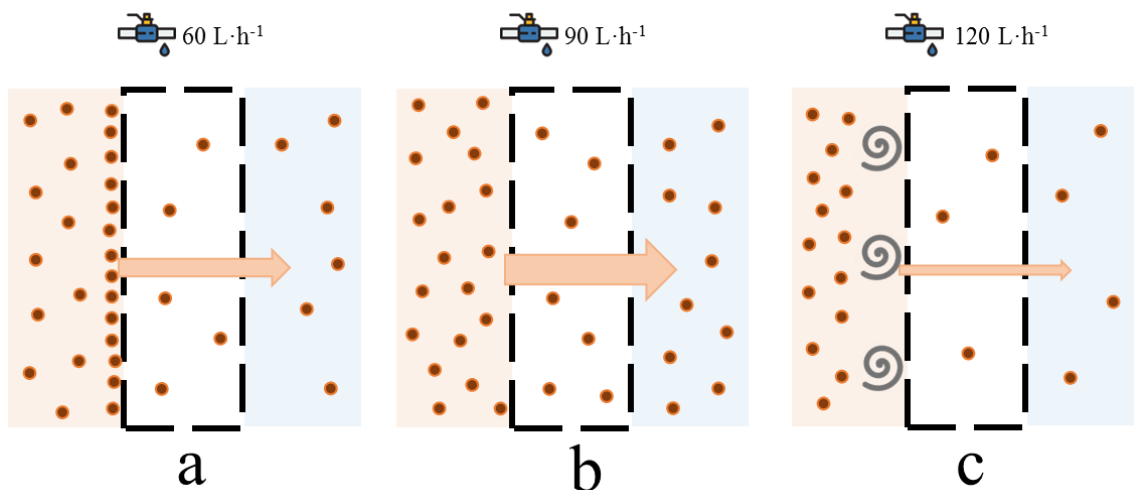


443 **Fig. 5.** HA diffusion in AGMD and WGMD because of temperature. Low temperatures imply a
 444 low particle speed and therefore, less diffusivity through the boundary layer (a). Higher
 445 temperatures assisted HA flux by improving diffusion of accumulated HA at the membrane
 446 surface (b). Permeate side temperature increase implies a HA concentration polarization
 447 decrease (c).
 448

449
 450 HA flux trend for flow rates tests can be explained by three different process as is illustrated in
 451 Fig.6. Firstly, at lower flow rate and cross flow velocity (2.28 cm s^{-1}), concentration polarization
 452 and boundary layer phenomena are significant leading to high HA concentration at the surface
 453 under relatively quiescent conditions. In this way, most of molecules and colloids of HA were
 454 deposited on the membrane surface, inhibiting HA diffusion through the membrane. For
 455 AGMD, at lower CFV (2.28 and 2.86 cm s^{-1}), lower HA flux compared to WGMD was
 456 obtained, as it was shown in Figure 3. These results suggested a CFV influence by concentration
 457 polarization and boundary layer phenomena. Thus, at low CFV, the residence time of HA on the
 458 membrane surface is longer. Therefore, with low velocity, higher concentration polarization, as
 459 well as a higher AGMD resistance to mass transfer, this resulted in a lower HA diffusion in this

460 MD configuration. Nevertheless, in WGMD, as a result of lower mass resistance, the HA
461 diffuses more easily to permeate under the same experimental conditions.

462 As the flow and CFV increased, the feed water mixture was increasingly homogeneous. For this
463 reason, the concentration polarization and associated boundary layer and HA fouling layer
464 phenomena were weakened, and HA diffusion to permeate reached a maximum at 90 L h^{-1} .
465 From this point, although the mixture is homogeneous at higher flow rates, HA flux dropped
466 noticeably at CFV of 4.00 and 4.57 cm s^{-1} . The latter process suggests the influence of shear
467 forces, which complicate HA transport to the membrane surface. It appears some accumulation
468 within the boundary layer is needed for HA flux to occur. With too much mixing and the
469 surface condition approaching the bulk solution, HA flux becomes reduced.



470

471 **Fig. 6.** Influence of the flow rates in HA diffusion for AGMD and WGMD. Predominance of
472 boundary layer phenomena and concentration by polarization (a). Complete mixture of feed
473 cycle, reaching the maximum diffusion (b). Shear forces play an important role at higher
474 flow rates (c).

475

476 To date, only a few studies have detected HA in permeate and their migration through the
477 membrane in DCMD. According to Meng et al (Meng et al., 2014), the process involves HA
478 adsorption-desorption onto the membrane surface, because of amphiphilic nature of HA. Thus,
479 HA migrates through the membrane pores by hydrogen bonding between water vapor and
480 humic molecules. This process suggests a dependence between migration mechanism and vapor
481 pressure and therefore, with the total flux for DCMD.

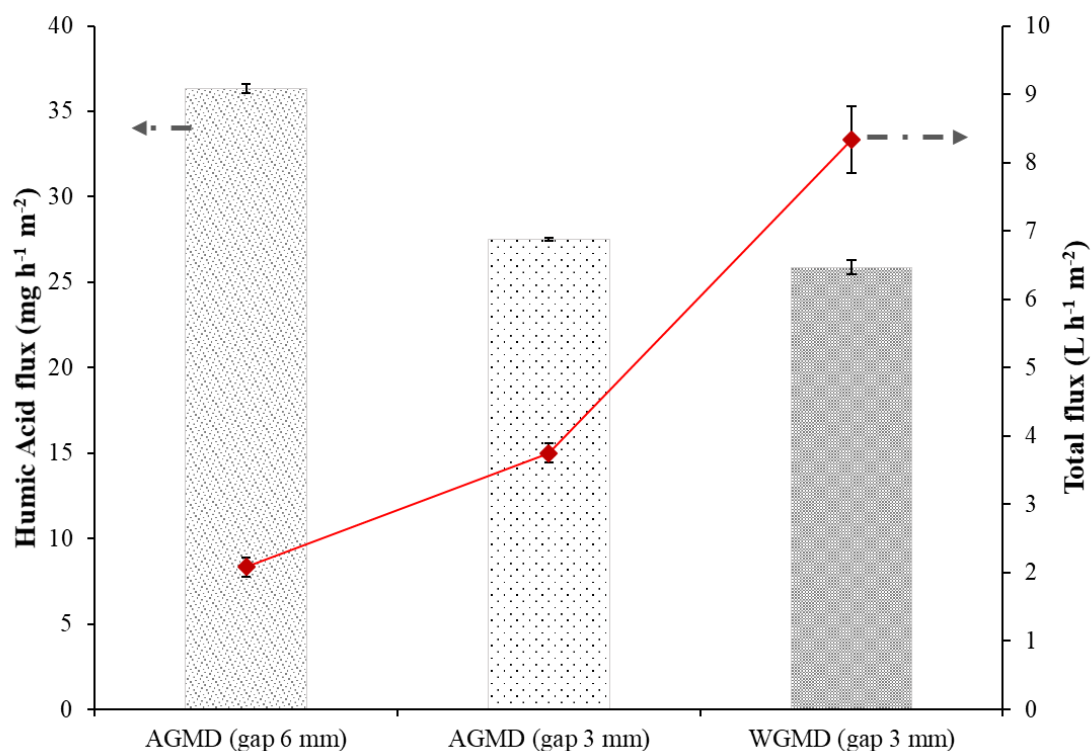
482 According to the results obtained for all tests carried out in this work and diffusion models
483 suggested, HA behavior based on diffusion is proposed for AGMD and WGMD. The diffusion
484 mechanism is independent of total flux and consequently, vapor pressure as well. AGMD and
485 WGMD have been used with the purpose of analyzing an isolated permeate, avoiding the
486 dilution effect in DCMD and therefore, not underestimating the amount of HA or NOM present
487 in permeate.

488 *3.5. Complementary studies*

489 *3.5.1. Double gap width for AGMD*

490 Following our finding earlier where HA flux occurred in AGMD as well as WGMD, water
491 bridges have been proposed by which HA could diffuse into permeate. These water bridges can
492 play an important role in this phenomenon, because of an additional sweeping effect of the
493 membrane cold side (Warsinger et al., 2018).

494 In relation to this suggestion, an additional frame was installed in order to double the gap size to
495 6 mm. Thus, a significant decrease in both total and HA fluxes could be expected. In this regard,
496 as it can be seen in Fig.7, while the total flux dropped noticeably, the HA flux detected was
497 greater (around 36%) than that obtained for 3 mm gap. Although a wider gap implied less water
498 bridging as well as total flux drop, slightly increased HA flux was obtained. These results
499 suggest that HA flux is not relying on total flux, and HA diffuses through the membrane in any
500 case. In addition, HA flux increase may be due to new conditions for wider gap as for example,
501 a favorable change in the temperature profile for HA diffusion. For example, at lower fluxes,
502 temperature polarization will be lower leading to larger temperature differences over the
503 membrane. As concluded earlier, the higher temperature on the feed side assisted HA flux by
504 improving its ability to diffuse through boundary layers containing accumulated HA at the
505 membrane surface which could also be eliminated by increasing cross flow (but only up to a
506 certain point).



507

508 **Fig. 7.** HA flux obtained for different gap tests. Total flux is represented by the lines with the
 509 values indicated on the secondary axis. Feed and cooling temperatures: 70°C and 18°C,
 510 respectively. Feed and cooling cycle flow rate: 90 L h⁻¹. Feed water: Deionized water and 50 mg
 511 L⁻¹ HA to avoid influence of salts and high HA concentrations. PTFE membrane with an
 512 effective area of 0.018 m². Due to low errors on some points, error bars cannot be seen.

513

514 3.5.2. HA preliminary characterization

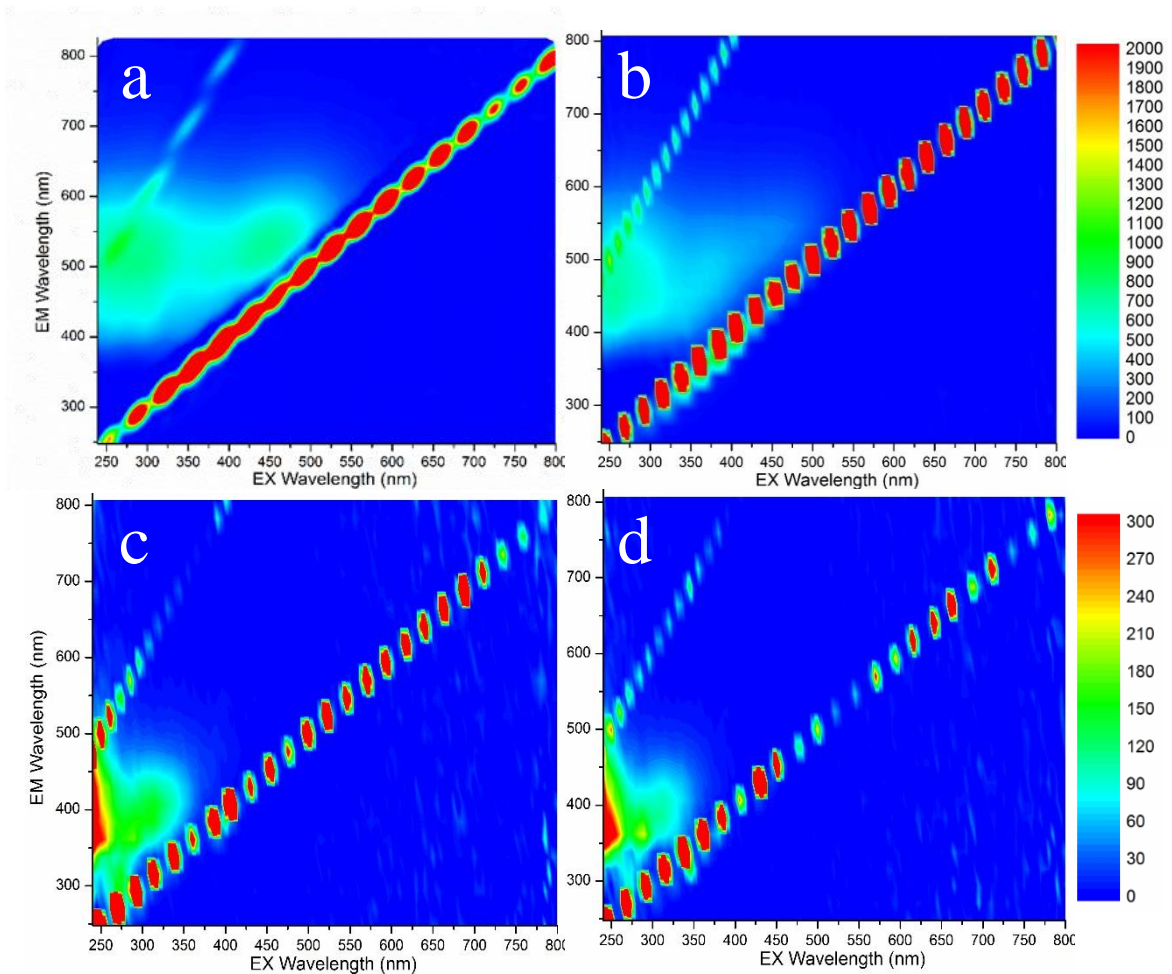
515 Using appropriate calibration curves for UV spectrometer and TOC analyzer, a good correlation
 516 was achieved for the synthetic water. This means that the absorbance could be known from the
 517 NPOC value and, therefore, the concentration of HA in the sample, indistinctly. Errors using the
 518 correlation between both techniques were less than 10%, with an average value of 7%. It is
 519 important to underline that different high and low range HA calibration curves were applied in
 520 order to cover the entire range of concentrations.

521 On the contrary, when these correlation equations were applied for UV spectrophotometer and
 522 TOC analyzer in permeate samples, errors obtained were above 87%. In addition, the
 523 absorbance values obtained in the permeate samples did not correspond to the absorbance that
 524 would have a feed water with the same concentration of HA measured with TOC analyzer. For

525 these reasons, a profile change in the HA molecule is suggested, since it seems that the HS
526 found in permeate absorb UV differently and therefore, they have different properties to the
527 original HS contained in the feed water.

528 The composition differences of HA in feed and permeate was also analyzed using fluorescence
529 spectrophotometry. Nevertheless, Excitation – Emission Matrix (EEM) fluorescence spectra can
530 be altered by pH and salt concentrations in the sample. In order to study the possible saline
531 interferences and differences between feed and permeate EEM spectra (Fig.8), fluorescence
532 measurements were made using different concentrations of HA in deionized water without salts,
533 as well as synthetic water (MD feed water) at different concentrations of HA. In all these
534 measurements, EEM spectra similar to each other were obtained. In Fig. 8a an EEM spectrum of
535 HA in deionized water (without added salts) is shown.

536 In Fig.8.b, an EEM fluorescence spectrum obtained from a synthetic water feed sample is
537 shown. This spectrum presents typical values for a standard HA, showing two Ex/Em peaks
538 around 250-350/450 nm (Rodríguez et al., 2014). High similarities between the EEM spectra of
539 synthetic water feed and HA with deionized water are observed. Both EEM spectra showed the
540 same profile as well as the peaks related to HA. Additionally, EEM spectra for AGMD and
541 WGMD permeate samples are shown in Fig. 8c and 8d, respectively. The spectra obtained for
542 the permeate samples in both MD configurations are very similar to each other, showing a
543 maximum Ex/Em peak around 250/350-400 nm. Although these permeate EEM spectra showed
544 fluorescence characteristics corresponding to humic acid-like substances (Wang et al., 2009),
545 clear differences in relation to the feed EEM spectrum and also, with HA in deionized water
546 EEM spectrum were observed. These results suggest and confirm a change in the HA profile
547 diffused through the membrane, as was previously proposed with the UV spectrometer
548 measurements.



549

550 **Fig. 8. a.** EEM spectrum for HA in deionized water; **b.** EEM spectrum for synthetic feed water
 551 sample; **c.** EEM spectrum for AGMD permeate sample; **d.** EEM spectrum for WGMD permeate
 552 sample.

553

554 4. Conclusions

555 Tests with different operating temperatures, flow rates and MD membranes were performed in
 556 order to study HA behavior, using AGMD and WGMD configurations. Non-volatile compounds
 557 have been detected in permeate, and humic flux through the membrane was affected by feed and
 558 cooling temperatures, boundary layers phenomenon, polarization concentration and shear
 559 forces. In addition, omniphobic PE membrane showed better HA rejection than the other
 560 membranes tested. In this way, MD membrane could play an important role in MD, which
 561 suggests that MD membrane is not only a passive element in the process. The same HA or

562 NOM behavior was obtained using both seawater and synthetic water. Therefore, a HA and
563 NOM diffusion mechanism is proposed for AGMD and WGMD configurations.

564 On the other hand, a sweeping effect on the membrane cold side was detected in AGMD
565 because of the frame, which separates the membrane and the cooling plate, acts as an
566 intermediate condenser. Humic flux in AGMD could be similar as in WGMD because of this
567 sweeping effect of the membrane.

568 Finally, a preliminary characterization of HA in MD permeate was carried out. HA differences
569 in permeate and feed were detected. In this way, it is necessary to go in depth with HA
570 characterization of MD permeate in order to analyze the OM complexation capacity and the
571 transport of undesired compounds through the membrane.

572

573 **Acknowledgments**

574 Authors want to acknowledge to University of Cadiz for supporting a predoctoral contract
575 within the Researcher Personnel Training Program (ref. 2015-036/PU/EPIF-FPI-CT/CP).

576 Leslie Naidoo of Australian Textile Mills is acknowledged for providing the laminated PU-
577 PTFE membranes used in this study.

578 Bart Nelemans of Aquastill is acknowledged for providing the hydrophobic PE and oleophobic
579 PE membranes used in this study.

580

581 **References**

582 Alkhudhiri, A., Darwish, N., Hilal, N., 2012a. Membrane distillation: A comprehensive review.
583 Desalination 287, 2–18. <https://doi.org/10.1016/j.desal.2011.08.027>

584 Alkhudhiri, A., Darwish, N., Hilal, N., 2012b. Treatment of high salinity solutions: Application
585 of air gap membrane distillation. Desalination 287, 55–60.

586 <https://doi.org/10.1016/j.desal.2011.08.056>

587 Alkhudhiri, A., Hilal, N., 2017. Air gap membrane distillation: A detailed study of high saline
588 solution. *Desalination* 403, 179–186. <https://doi.org/10.1016/j.desal.2016.07.046>

589 Amaya-Vías, D., Nebot, E., López-Ramírez, J.A., 2018. Comparative studies of different
590 membrane distillation configurations and membranes for potential use on board cruise
591 vessels. *Desalination* 429, 44–51. <https://doi.org/10.1016/J.DESAL.2017.12.008>

592 Anand, A., Unnikrishnan, B., Mao, J.Y., Lin, H.J., Huang, C.C., 2018. Graphene-based
593 nanofiltration membranes for improving salt rejection, water flux and antifouling—A
594 review. *Desalination* 429, 119–133. <https://doi.org/10.1016/j.desal.2017.12.012>

595 Attia, H., Alexander, S., Wright, C.J., Hilal, N., 2017a. Superhydrophobic electrospun
596 membrane for heavy metals removal by air gap membrane distillation (AGMD).
597 *Desalination* 420, 318–329. <https://doi.org/10.1016/j.desal.2017.07.022>

598 Attia, H., Osman, M.S., Johnson, D.J., Wright, C., Hilal, N., 2017b. Modelling of air gap
599 membrane distillation and its application in heavy metals removal. *Desalination* 424, 27–
600 36. <https://doi.org/10.1016/j.desal.2017.09.027>

601 Biel-Maeso, M., Baena-Nogueras, R.M., Corada-Fernández, C., Lara-Martín, P.A., 2018.
602 Occurrence, distribution and environmental risk of pharmaceutically active compounds
603 (PhACs) in coastal and ocean waters from the Gulf of Cadiz (SW Spain). *Sci. Total*
604 *Environ.* 612, 649–659. <https://doi.org/10.1016/J.SCITOTENV.2017.08.279>

605 Bond, T., Goslan, E.H., Parsons, S.A., Jefferson, B., 2012. A critical review of trihalomethane
606 and haloacetic acid formation from natural organic matter surrogates. *Environ. Technol.*
607 *Rev.* 1, 93–113. <https://doi.org/10.1080/09593330.2012.705895>

608 Chowdhury, S., Khan, N., Kim, G.-H., Harris, J., Longhurst, P., Bolan, N.S., 2016. Zeolite for
609 Nutrient Stripping From Farm Effluents, in: *Environmental Materials and Waste*. Elsevier,
610 pp. 569–589. <https://doi.org/10.1016/B978-0-12-803837-6.00022-6>

- 611 Criscuoli, A., Carnevale, M.C., 2015. Desalination by vacuum membrane distillation: The role
612 of cleaning on the permeate conductivity. *Desalination* 365, 213–219.
613 <https://doi.org/10.1016/J.DESAL.2015.03.003>
- 614 Cui, Z., Zhang, Y., Li, X., Wang, X., Wang, Z., Zhao, S., 2018. Optimization of novel
615 composite membranes for water and mineral recovery by vacuum membrane distillation.
616 *Desalination* 440, 39–47. <https://doi.org/10.1016/J.DESAL.2017.11.040>
- 617 Damtie, M.M., Kim, B., Woo, Y.C., Choi, J.-S., 2018. Membrane distillation for industrial
618 wastewater treatment: Studying the effects of membrane parameters on the wetting
619 performance. *Chemosphere* 206, 793–801.
620 <https://doi.org/10.1016/J.CHEMOSPHERE.2018.05.070>
- 621 Dow, N., Gray, S., Li, J. de, Zhang, J., Ostarcevic, E., Liubinas, A., Atherton, P., Roeszler, G.,
622 Gibbs, A., Duke, M., 2016. Pilot trial of membrane distillation driven by low grade waste
623 heat: Membrane fouling and energy assessment. *Desalination* 391, 30–42.
624 <https://doi.org/10.1016/j.desal.2016.01.023>
- 625 Duong, H.C., Chuai, D., Woo, Y.C., Shon, H.K., Nghiem, L.D., Sencadas, V., 2018. A novel
626 electrospun, hydrophobic, and elastomeric styrene-butadiene-styrene membrane for
627 membrane distillation applications. *J. Memb. Sci.* 549, 420–427.
628 <https://doi.org/10.1016/J.MEMSCI.2017.12.024>
- 629 Duong, H.C., Duke, M., Gray, S., Cooper, P., Nghiem, L.D., 2016. Membrane scaling and
630 prevention techniques during seawater desalination by air gap membrane distillation.
631 *Desalination* 397, 92–100. <https://doi.org/10.1016/j.desal.2016.06.025>
- 632 Essalhi, M., Khayet, M., 2015. Fundamentals of membrane distillation, in: *Pervaporation,*
633 *Vapour Permeation and Membrane Distillation.* Elsevier, pp. 277–316.
634 <https://doi.org/10.1016/B978-1-78242-246-4.00010-6>
- 635 Francis, L., Ghaffour, N., Alsaadi, A.A., Amy, G.L., 2013. Material gap membrane distillation:

636 A new design for water vapor flux enhancement. *J. Memb. Sci.* 448, 240–247.
637 <https://doi.org/10.1016/j.memsci.2013.08.013>

638 García-Fernández, L., Khayet, M., García-Payo, M.C., 2015. Membranes used in membrane
639 distillation: Preparation and characterization, Pervaporation, Vapour Permeation and
640 Membrane Distillation: Principles and Applications. [https://doi.org/10.1016/B978-1-](https://doi.org/10.1016/B978-1-78242-246-4.00011-8)
641 [78242-246-4.00011-8](https://doi.org/10.1016/B978-1-78242-246-4.00011-8)

642 Ghaffour, N., Missimer, T.M., Amy, G.L., 2013. Technical review and evaluation of the
643 economics of water desalination: Current and future challenges for better water supply
644 sustainability. *Desalination* 309, 197–207. <https://doi.org/10.1016/J.DESAL.2012.10.015>

645 Giovanela, M., Crespo, J.S., Antunes, M., Adamatti, D.S., Fernandes, A.N., Barison, A., da
646 Silva, C.W.P., Guégan, R., Motelica-Heino, M., Sierra, M.M.D., 2010. Chemical and
647 spectroscopic characterization of humic acids extracted from the bottom sediments of a
648 Brazilian subtropical microbasin. *J. Mol. Struct.* 981, 111–119.
649 <https://doi.org/10.1016/J.MOLSTRUC.2010.07.038>

650 Giovanela, M., Parlanti, E., Soriano-Sierra, E.J., Soldi, M.S., Sierra, M.M.D., 2004. Elemental
651 compositions, FT-IR spectra and thermal behavior of sedimentary fulvic and humic acids
652 from aquatic and terrestrial environments, *Geochemical Journal*.

653 González, D., Amigo, J., Suárez, F., 2017. Membrane distillation : Perspectives for sustainable
654 and improved desalination. *Renew. Sustain. Energy Rev.* 80, 238–259.
655 <https://doi.org/10.1016/j.rser.2017.05.078>

656 Guillen-Burrieza, E., Ruiz-Aguirre, A., Zaragoza, G., Arafat, H.A., 2014. Membrane fouling
657 and cleaning in long term plant-scale membrane distillation operations. *J. Memb. Sci.* 468,
658 360–372. <https://doi.org/10.1016/j.memsci.2014.05.064>

659 Han, L., Xiao, T., Zen, Y., Fane, A.G., Wei, J., 2017. Contaminant rejection in the presence of
660 humic acid by membrane distillation for surface water treatment. *J. Memb. Sci.* 541, 291–

661 299. <https://doi.org/10.1016/j.memsci.2017.07.013>

662 Herce-Sesa, B., López-López, J.A., Moreno, C., 2018. Multi-elemental ionic liquid-based
663 solvent bar micro-extraction of priority and emerging trace metallic pollutants (Cd, Ag,
664 Pd) in natural waters. *J. Hazard. Mater.* <https://doi.org/10.1016/J.JHAZMAT.2018.02.024>

665 Jermann, D., Pronk, W., Meylan, S., Boller, M., 2007. Interplay of different NOM fouling
666 mechanisms during ultrafiltration for drinking water production. *Water Res.* 41, 1713–
667 1722. <https://doi.org/10.1016/J.WATRES.2006.12.030>

668 Khalifa, A.E., 2015. Water and air gap membrane distillation for water desalination - An
669 experimental comparative study. *Sep. Purif. Technol.* 141, 276–284.
670 <https://doi.org/10.1016/j.seppur.2014.12.007>

671 Khalifa, A.E., Alawad, S.M., 2018. Air gap and water gap multistage membrane distillation for
672 water desalination. *Desalination* 437, 175–183.
673 <https://doi.org/10.1016/J.DESAL.2018.03.012>

674 Khayet, M., 2011. Membranes and theoretical modeling of membrane distillation: A review.
675 *Adv. Colloid Interface Sci.* 164, 56–88. <https://doi.org/10.1016/j.cis.2010.09.005>

676 Khayet, M., Velázquez, A., Mengual, J.I., 2004. Direct contact membrane distillation of humic
677 acid solutions. *J. Memb. Sci.* 240, 123–128. <https://doi.org/10.1016/j.memsci.2004.04.018>

678 Kim, J., Hong, S., 2018. A novel single-pass reverse osmosis configuration for high-purity
679 water production and low energy consumption in seawater desalination. *Desalination* 429,
680 142–154. <https://doi.org/10.1016/j.desal.2017.12.026>

681 Kolokassidou, C., Pashalidis, I., Costa, C.N., Efstathiou, A.M., Buckau, G., 2007. Thermal
682 stability of solid and aqueous solutions of humic acid. *Thermochim. Acta* 454, 78–83.
683 <https://doi.org/10.1016/j.tca.2006.12.022>

684 Lipczynska-Kochany, E., 2018. Humic substances, their microbial interactions and effects on
685 biological transformations of organic pollutants in water and soil: A review. *Chemosphere*

686 202, 420–437. <https://doi.org/10.1016/J.CHEMOSPHERE.2018.03.104>

687 Liu, S., Lim, M., Fabris, R., Chow, C., Chiang, K., Drikas, M., Amal, R., 2008. Removal of
688 humic acid using TiO₂ photocatalytic process – Fractionation and molecular weight
689 characterisation studies. *Chemosphere* 72, 263–271.
690 <https://doi.org/10.1016/J.CHEMOSPHERE.2008.01.061>

691 Meng, S., Ye, Y., Mansouri, J., Chen, V., 2014. Fouling and crystallisation behaviour of
692 superhydrophobic nano-composite PVDF membranes in direct contact membrane
693 distillation. *J. Memb. Sci.* 463, 102–112. <https://doi.org/10.1016/j.memsci.2014.03.027>

694 Miller, J.N., Miller, J.C., Maté Jiménez, C., Izquierdo Hornillos, R., 2002. *Estadística y*
695 *quimiometría para química analítica*. Prentice Hall.

696 Mostafa, M.G., Zhu, B., Cran, M., Dow, N., Milne, N., Desai, D., Duke, M., 2017. Membrane
697 distillation of meat industry effluent with hydrophilic polyurethane coated
698 polytetrafluoroethylene membranes. *Membranes (Basel)*. 7, 55.
699 <https://doi.org/10.3390/membranes7040055>

700 Myat, D.T., Mergen, M., Zhao, O., Stewart, M.B., Orbell, J.D., Gray, S., 2012. Characterisation
701 of organic matter in IX and PACl treated wastewater in relation to the fouling of a
702 hydrophobic polypropylene membrane. *Water Res.* 46, 5151–5164.
703 <https://doi.org/10.1016/j.watres.2012.06.054>

704 Naidu, G., Jeong, S., Kim, S.J., Kim, I.S., Vigneswaran, S., 2014. Organic fouling behavior in
705 direct contact membrane distillation. *Desalination* 347, 230–239.
706 <https://doi.org/10.1016/j.desal.2014.05.045>

707 Naidu, G., Jeong, S., Vigneswaran, S., 2015. Interaction of humic substances on fouling in
708 membrane distillation for seawater desalination. *Chem. Eng. J.* 262, 946–957.
709 <https://doi.org/10.1016/J.CEJ.2014.10.060>

710 Pal, P., Manna, A.K., 2010. Removal of arsenic from contaminated groundwater by solar-driven

711 membrane distillation using three different commercial membranes. *Water Res.* 44, 5750–
712 5760. <https://doi.org/10.1016/j.watres.2010.05.031>

713 Prisciandaro, M., Capocelli, M., Piemonte, V., Barba, D., 2016. Process analysis applied to
714 water reuse for a “closed water cycle” approach. *Chem. Eng. J.* 304, 602–608.
715 <https://doi.org/10.1016/J.CEJ.2016.06.134>

716 Qin, W., Xie, Z., Ng, D., Ye, Y., Ji, X., Gray, S., Zhang, J., 2018. Comparison of colloidal silica
717 involved fouling behavior in three membrane distillation configurations using PTFE
718 membrane. *Water Res.* 130, 343–352. <https://doi.org/10.1016/J.WATRES.2017.12.002>

719 Qtaishat, M., Khayet, M., Matsuura, T., 2009. Novel porous composite hydrophobic/hydrophilic
720 polysulfone membranes for desalination by direct contact membrane distillation. *J. Memb.*
721 *Sci.* 341, 139–148. <https://doi.org/10.1016/J.MEMSCI.2009.05.053>

722 Roccaro, P., Vagliasindi, F.G.A., Korshin, G. V., 2009. Changes in NOM Fluorescence Caused
723 by Chlorination and their Associations with Disinfection by-Products Formation. *Environ.*
724 *Sci. Technol.* 43, 724–729. <https://doi.org/10.1021/es801939f>

725 Rodríguez, F.J., Schlenger, P., García-Valverde, M., 2014. A comprehensive structural
726 evaluation of humic substances using several fluorescence techniques before and after
727 ozonation. Part I: Structural characterization of humic substances. *Sci. Total Environ.* 476–
728 477, 718–730. <https://doi.org/10.1016/J.SCITOTENV.2013.11.150>

729 Silva, T.L.S., Morales-Torres, S., Esteves, C.M.P., Ribeiro, A.R., Nunes, O.C., Figueiredo, J.L.,
730 Silva, A.M.T., 2018. Desalination and removal of organic micropollutants and
731 microorganisms by membrane distillation. *Desalination* 437, 121–132.
732 <https://doi.org/10.1016/J.DESAL.2018.02.027>

733 Villalobos García, J., Dow, N., Milne, N., Zhang, J., Naidoo, L., Gray, S., Duke, M., 2018.
734 Membrane Distillation Trial on Textile Wastewater Containing Surfactants Using
735 Hydrophobic and Hydrophilic-Coated Polytetrafluoroethylene (PTFE) Membranes.

736 Membranes (Basel). 8, 31. <https://doi.org/10.3390/membranes8020031>

737 Voulvoulis, N., 2018. Water reuse from a circular economy perspective and potential risks from
738 an unregulated approach. *Curr. Opin. Environ. Sci. Heal.* 2, 32–45.
739 <https://doi.org/10.1016/j.coesh.2018.01.005>

740 Wagner, M., Schmidt, W., Imhof, L., Grübel, A., Jähn, C., Georgi, D., Petzoldt, H., 2016.
741 Characterization and quantification of humic substances 2D-Fluorescence by usage of
742 extended size exclusion chromatography. *Water Res.* 93, 98–109.
743 <https://doi.org/10.1016/J.WATRES.2016.01.050>

744 Wang, K., Hou, D., Wang, J., Wang, Z., Tian, B., Liang, P., 2018. Hydrophilic surface coating
745 on hydrophobic PTFE membrane for robust anti-oil-fouling membrane distillation. *Appl.*
746 *Surf. Sci.* 450, 57–65. <https://doi.org/10.1016/J.APSUSC.2018.04.180>

747 Wang, Z., Wu, Z., Tang, S., 2009. Characterization of dissolved organic matter in a submerged
748 membrane bioreactor by using three-dimensional excitation and emission matrix
749 fluorescence spectroscopy. *Water Res.* 43, 1533–1540.
750 <https://doi.org/10.1016/j.watres.2008.12.033>

751 Warsinger, D.M., Swaminathan, J., Morales, L.L., Lienhard V, J.H., 2018. Comprehensive
752 condensation flow regimes in air gap membrane distillation: Visualization and energy
753 efficiency. *J. Memb. Sci.* 555, 517–528. <https://doi.org/10.1016/j.memsci.2018.03.053>

754 Wijekoon, K.C., Hai, F.I., Kang, J., Price, W.E., Cath, T.Y., Nghiem, L.D., 2014. Rejection and
755 fate of trace organic compounds (TrOCs) during membrane distillation. *J. Memb. Sci.* 453,
756 636–642.

757 Woo, Y.C., Tijing, L.D., Shim, W.-G., Choi, J.-S., Kim, S.-H., He, T., Drioli, E., Shon, H.K.,
758 2016. Water desalination using graphene-enhanced electrospun nanofiber membrane via
759 air gap membrane distillation. *J. Memb. Sci.* 520, 99–110.
760 <https://doi.org/10.1016/J.MEMSCI.2016.07.049>

761 Xu, J., Singh, Y.B., Amy, G.L., Ghaffour, N., 2016. Effect of operating parameters and
762 membrane characteristics on air gap membrane distillation performance for the treatment
763 of highly saline water. *J. Memb. Sci.* 512, 73–82.
764 <https://doi.org/10.1016/j.memsci.2016.04.010>

765 Zheng, R., Chen, Y., Wang, J., Song, J., Li, X.-M., He, T., 2018. Preparation of omniphobic
766 PVDF membrane with hierarchical structure for treating saline oily wastewater using
767 direct contact membrane distillation. *J. Memb. Sci.* 555, 197–205.
768 <https://doi.org/10.1016/J.MEMSCI.2018.03.041>

769 Ziolkowska, J.R., Reyes, R., 2016. Impact of socio-economic growth on desalination in the US.
770 *J. Environ. Manage.* 167, 15–22. <https://doi.org/10.1016/J.JENVMAN.2015.11.013>

771

Declaration of interests

The authors declare that they have no known competing financial interests or personal relationships that could have appeared to influence the work reported in this paper.

The authors declare the following financial interests/personal relationships which may be considered as potential competing interests: